Atmospheric Dynamics II
ASME 434
Department of Physics
NC A&T State University

Prof. Yuh-Lang Lin
ylin@ncat.edu
https://mesolab.org

11. Isolated Convective Storms

(Based on Ch. 8, "Mesoscale Dynamics", by Y.-L. Lin 2007)

11. Isolated Convective Storms

11.1 Dynamics of single-cell storms and downbursts
11.2 Dynamics of multicell storms
11.3 Effects of Shear and Buoyancy
11.4 Dynamics of Supercell Storms
11.5 Tornado Dynamics

11. Isolated convective storms

- Isolated convective storms are generally considered to be cumulonimbus clouds that produce thunder and lightning, heavy rainfall, wind gusts, and occasionally large hail and tornadoes.

- Understanding the dynamics of isolated convective storms is important because these storms form the building blocks of much more complicated mesoscale convective systems, such as squall lines and mesoscale convective complexes.

- Aside from their hazards to society, cumulonimbus clouds also play an important role in:

  - Providing needed rainfall to many regions of the Earth
  - Participating in the general circulation by transporting moisture and sensible and latent heat to the upper troposphere and lower stratosphere, and
  - Composing a significant part in the radiative budgets of the atmosphere.

- Various methods have been proposed to classify different storm types according to their internal structure, rainfall intensity, potential severity, longevity, and propagation properties.

  In this text, we adopt standard nomenclature and categorize them as single cell, multicell and supercell storms.

- The ordinary, *single-cell storm* consists of only one convective cell, which is short-lived and often associated with weak vertical shear.

- When a cluster of single cells at various stages exists simultaneously within a storm, it is called a *multicell storm*. Multicell storms normally exist in an environment with moderate shear, and have

longer lifetimes than single-cell storms since new cells continue to develop along the gust front as the older cells are dissipating.

- A *supercell storm* consists of a single rotating updraft, which often exists in an environment with strong shear and has a lifetime much longer than a single-cell storm, often lasting for several hours. Supercell thunderstorms produce the majority of severe weather.

- Since the characteristics of these three types of isolated convective storms have been discussed in detail in several textbooks and review articles on cloud dynamics, this chapter will focus on the basic dynamics of convective storms and important recent findings in the field.

11.1 Dynamics of single-cell storms and downbursts

- Compared to multicell and supercell storms, the dynamics of single-cell storms are better understood partially due to their less complicated characteristics and the wealth of information from earlier field observations.

- The basic characteristics of a single-cell storm may be summarized as the following:
  (1) Composed of one single updraft or updraft-downdraft pair.
  (2) The updraft may penetrate the tropopause and have a horizontal scale on the order of several kilometers.
  (3) The environmental vertical wind shear is weak, often smaller than 10 ms^{-1} in the lowest 4 km.
  (4) The storm normally moves with the mean wind in the lower to middle troposphere.
  (5) The lifetime is on the order of 30 minutes.
  (6) The storm is usually not strong enough to produce severe weather but is occasionally accompanied by thunder and lightning.

- The structure and life cycle of a single-cell storm are sketched in Fig. 8.1.

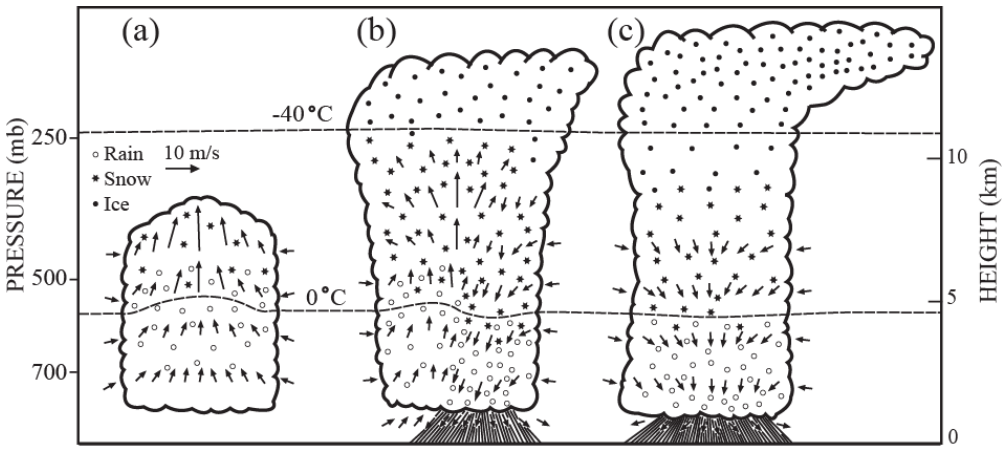

Fig. 8.1: Three stages for the life cycle of a single-cell storm: (a) developing stage, (b) mature stage, and (c) dissipation stage. (Adapted after Byers and Braham 1949) [Lin 2007]

- A single-cell storm is often accompanied by thunder and lightning and is referred to as an *air mass thunderstorm*.

- This type of thunderstorm was the target of the Thunderstorm Project, which was held over Florida and Ohio during the late 1940s.

Three distinctive stages are identified for a single-cell storm:
(a) *developing stage*,
(b) *mature stage*, and
(c) *dissipating stage*.

The *developing stage* is characterized by

- A towering cumulus cloud consists entirely of a warm, strong updraft (Fig. 8.1a).
- This updraft develops in a weak shear environment and its velocity may exceed 10 ms^{-1}.
- Entrainment occurs at the lateral cloud boundaries.
- At this stage, precipitation starts to form as raindrops or ice particles in the upper portion of the cumulus cloud, however no significant rainfall occurs in the subcloud layer.

During the *mature stage*,

- The cloud continues to grow, and precipitation particles begin to fall below the cloud base (Fig. 8.1b).
- Evaporation from falling precipitation particles cools the unsaturated air below the cloud base, thus forming a cold pool which, hydrostatically, leads to a mesoscale region of high pressure (*mesohigh*) near the surface.
- The maximum vertical velocity of the storm is located at the middle of the cloud.
- Detrainment occurs above middle of the cloud while divergence occurs near the cloud top.
- Weak vertical wind shear causes precipitation particles to fall directly into the updraft, which results in a downdraft that effectively shuts off the updraft.

The above triggers the *dissipation stage*.

- Single-cell storms are usually not strong and do not last long enough to produce severe weather.

- The Thunderstorm Project observations also found that only 20% of the condensed water in the updraft actually reaches the ground. This means that on average the *precipitation efficiency*, i.e. the ratio of total precipitation to total available moisture of a cloud system, for air mass thunderstorms is low.

- On the other hand, the precipitation efficiency of a squall line may in average reach as high as 50% due to less entrainment and a longer lifetime (Newton 1966). Larger precipitation efficiency is often associated with: (a) a weaker wind shear, (b) a longer lifetime of a cloud system, (c) a lower cloud base, (d) a larger cloud base area, (e) a larger cloud base mixing ratio, and (f) a smaller CIN (e.g., Market et al. 2003).

[Cloud merging]

- The most intense and persistent convective clouds, as has been well documented, are often associated with the merging of two or more adjacent convective cells.

- *Cloud merging* may increase cloud size significantly, resulting in more rainfall than in unmerged cells.

- Cumulus downdrafts and their associated cold outflow have often been proposed to play a critical role in the cloud merging process (Fig. 8.2).

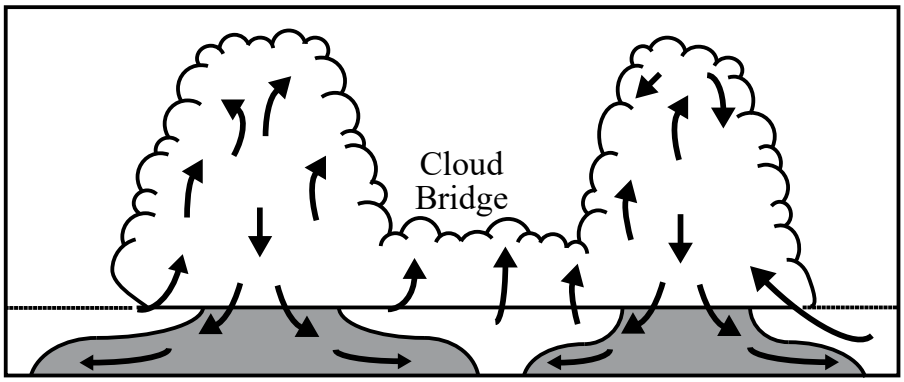

Fig. 8.2: A conceptual model of cloud merging through downdraft interaction in the case of light wind and weak shear. (Adapted after Simpson et al. 1980) [Lin 2007]

- The downdrafts produce cold outflows, which approach each other and collide to form a *cloud bridge*. New towers then surge upward from the bridge to fill the gap.

- The process of outflow bridge formation often precedes the radar echo merger and therefore cannot be detected through radar echo analysis.

- In addition to the cloud merging process, cold outflow also plays an essential role in the generation of new cells in multicell storms and the generation, maintenance, and propagation of

squall lines, as will be discussed in the rest of this chapter and in the next chapter.

[Downburst]

- Almost all intense convective storms are able to produce strong horizontal winds at the ground level. A *downburst* refers to a large area of damaging winds induced by a strong downdraft on or near the ground.
- The severe wind associated with downbursts and gust fronts is often referred to as a *straight-line wind* in order to distinguish it from the twisting nature of the damaging winds associated with tornadoes.
- Normally, a downburst covers a horizontal area with a diameter from less than 1 km to 10 km.
- Depending on the intensity and characteristics of the downburst, it may be further classified into: (a) *macroburst*: a downburst that occurs over a horizontal area greater than 4 km and lasts for 5 - 30 min; or (b) *microburst*: a downburst that occurs over a horizontal area less than 4 km and lasts for 2 – 5 min.
- The formation of a microburst may be classified into three stages: (1) developing stage; (2) touchdown stage; and (3) outburst stage. Figures 8.3a and 8.3b show an observed and numerically simulated microburst which occurred in Denver on 14 July 1982.

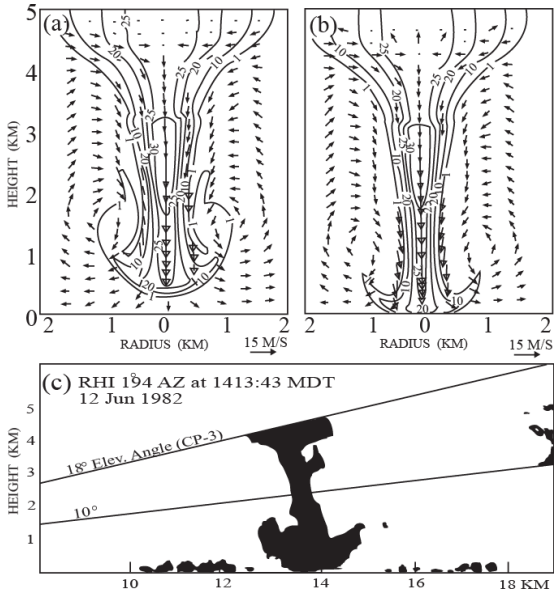

Fig. 8.3: The numerically simulated radar reflectivity and superimposed vector wind field for an idealized microburst that occurred in Denver on 14 July 1982 at (a) 22 min and (b) 23 min (Proctor 1989). The contour values are in units of dBZ. The funnel, shaft and arrow-head shapes of the simulated radar echo mimic those of an observed microburst as shown in (c), which was observed during the field experiment JAWS. (Adapted after Fujita and Wakimoto 1983) [Lin 2007]

- The microburst may be further classified into (Wakimoto 1985):

  (a) dry microburst: a microburst accompanied by little or no precipitation during the period of outflow and usually associated with virga from mid-level altocumuli or high-based cumulonimbi; and

  (b) wet microburst: a microburst often accompanied by heavy precipitation during the period of outflow and is usually associated with strong precipitation shafts from thunderstorms.

- The intense downdrafts produced within thunderstorms are mainly caused by the negative buoyancy of the air parcels. The negative buoyancy is produced by the cooling associated with the evaporation of raindrops and/or melting and sublimation of frozen precipitation hydrometeors as they fall through the subsaturated layer.

- Another primary cause of wet microburst generation is thought to be precipitation loading.

  Precipitation loading occurs in thunderstorms when the weight of excessive condensates within the cloud creates a downward force.

  This effect thereby either induces a downward current of air or enhances descending air within a downdraft.

  Observational studies of downdraft cores, however, show that in some cases the virtual temperature of the subsiding air can be relatively warm (e.g., Igau et al. 1999). Therefore, precipitation loading can serve to make the downdrafts negatively buoyant in these situations (Jorgensen and LeMone 1989).

- The physical processes leading to a downdraft within a convective storm are very different from those leading to an updraft. The formation of small (on the order of mm) hydrometeors results in an updraft temperature profile close to the saturated or supersaturated adiabatic lapse rate.

- On the other hand, small hydrometeors in a downdraft are quickly depleted by evaporation, which may lead to an unsaturated lapse rate through the release of latent heat. Thus, in order to accurately simulate a thunderstorm downdraft with a numerical model, consideration of the microphysical processes associated with liquid or solid condensate is of paramount importance.

- Figures 8.3a and 8.3b depict the radar reflectivity and superimposed vector wind field for a numerical simulation of an idealized microburst that occurred in Denver on 14 July 1982. This downburst was mainly produced by the cooling associated with melting snow.

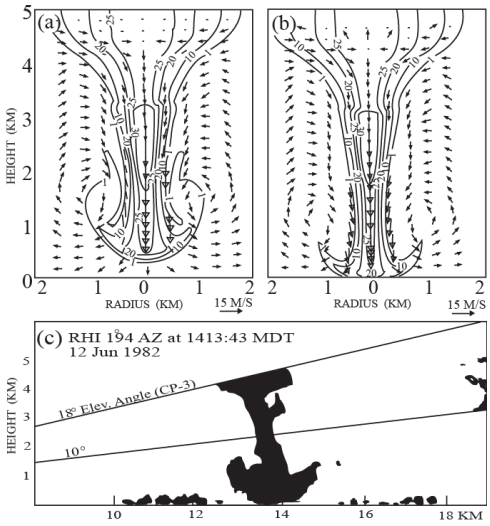

Fig. 3 (Lin 2007)

The three stages, i.e. *developing stage*, *touchdown stage*, and *outburst stage*, were well simulated by the numerical model.

During the earlier stages, the falling snow particles produced a radar echo which has been typical in other snow-produced downburst events.

The downburst base is formed by small rain droplets that are swept into the microburst's ring-vortex circulation (Figs. 8.3a-b).

Later, the base disappears as the *ring vortex* stretches outward behind the expanding outflow (Fig. 8.3c).

In a melting-induced downburst, the maximum radar reflectivity is often located at the melting level.

In this particular case, throughout the life cycle of the microburst, the maximum radar reflectivity due to melting snow is located about 2.4 km above ground.

- A majority of the outburst winds from outflow associated with microbursts are straight. Therefore, the streamlines of outburst winds spread out radially and do not rotate around the center of the outflow.

- However, some microbursts are associated with small-scale cyclonic circulations and the rotation of the microburst may strengthen or weaken it, depending upon the height of the minimum pressure perturbation.

- When the minimum pressure perturbation is located at or near the surface, it tends to strengthen the microburst; when it is located substantially above the surface, it tends to weaken the microburst.

11.2 Dynamics of multicell storms

- A multicell storm is composed of several convective cells throughout various stages of their life cycles.

- The existence of stronger shear in the environment prevents circulations associated with individual convective cells from interfering with each other, thus allowing the overall multicell storm system to last for several hours.

- The individual embedded cells are normally short-lived single cells that are generated by the quasi-steady updraft cell over the leading edge of the cold pool of outflow, i.e. the *gust front*.

- Normally, a new cell then forms in or near the gust front updraft, developing vertically and moving rearward within the front-to-rear jet.

  The *front-to-rear jet* is an ascending airstream from the low-level environmental inflow that resides above the subcloud cold pool and flows toward the rear portion of the storm and over the rear-to-front jet.

  The *rear-to-front jet* or *rear inflow* is the jet with low-θ_e air, flowing from the rear part of the storm into the rear part of the cold pool.

- The new cells are generated, develop, and are cut off from the gust front updraft in a discrete manner and in a periodic fashion every 10 - 15 minutes.

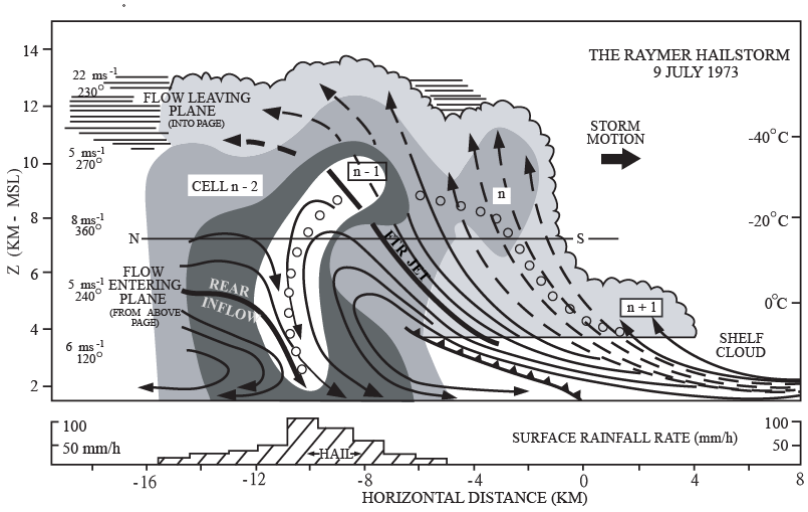

Fig. 8.4: A schematic diagram for a multicell storm on a vertical plane along the direction of storm's movement. This storm has been referred to as the Raymer hailstorm. A series of convective cells, denoted as n-2, n-1, n, and n+1, were generated at the gust front and moved to the left as they developed. The solid lines represent storm-relative streamlines on the vertical plane; the broken lines on the left and right sides of the figure represent flow into and out of the plane and flow remaining within a plane a few kilometers closer to the reader, respectively. FTR JET and RTF JET stand for front-to-rear jet and rear-to-front jet (rear inflow), respectively, and are denoted by thick streamlines. The open circles represent the trajectory of a hailstone during its growth from a small droplet at cloud base. (Adapted after Browning et al. 1976) [Lin 2007]

- Figure 8.4 shows a schematic diagram for a multicell storm in the vertical plane along the direction of storm's movement.

- The storm produced hail and is often referred to as the Raymer hailstorm, which occurred on 9 July 1973 at Raymer, Colorado.

- A series of convective cells, denoted as n-2, n-1, n, and n+1, were generated as the gust front propagated rightward.

- These four individual convective cells are at four different stages of their life cycles.

  Cell n-2 is in the decaying stage, which is characterized at most levels by weak downdrafts and a residual weak updraft in places aloft. Part

of the mature cell n-2 has already been converted into a vigorous downdraft.

Cell n-1 is in its mature stage, and has almost reached its maximum intensity.

Cell n is just starting to grow out of the shelf cloud. A *shelf cloud* is a low cloud that protrudes horizontally from a thunderstorm cloud, in association with a gust front.

A distinct new Cell n+1 forms as a shelf cloud about 15 minutes later.

Figure 8.5 shows a schematic diagram of individual cell movement within an ordinary multicell storm, which is often observed in the central USA.

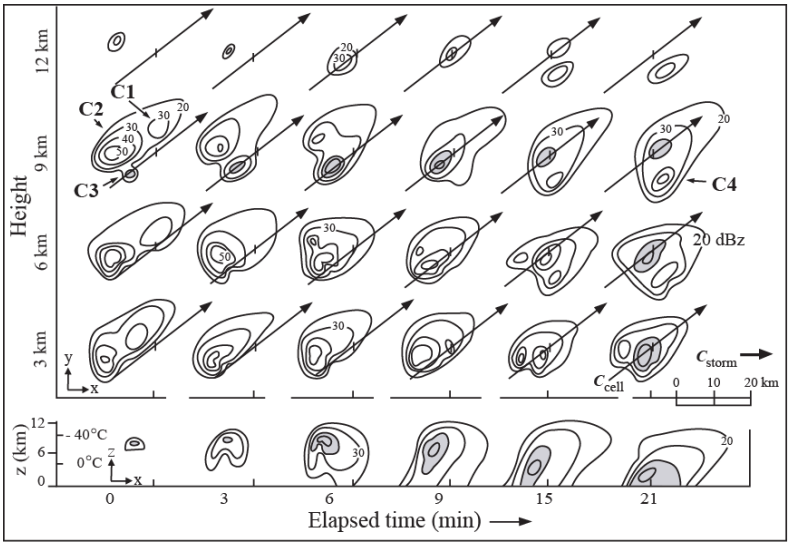

Fig. 8.5: Schematic diagram for the propagation and evolution of an ordinary multicell storm (Raymer hailstorm, Fig. 8.4). Both the horizontal and vertical radar reflectivity contours (at 10 dBZ intervals) are sketched. Horizontal cross-sections are illustrated for four altitudes at six different times. Individual cell motions are steered by a midlevel wind toward the northeast (denoted by $\boldsymbol{c}_{cell}$), while the entire storm moves towards the east (denoted by $\boldsymbol{c}_{storm}$). New convective cells, such as cells 3 and 4 (denoted as C3 and C4), are generated to the south of the storm against the low-level wind. (After Chisholm and Renick 1972) [Lin 2007]

[Fig. 8.5] New convective cells, such as Cells 3 and 4, are generated to the south of the multicell storm and against the low-level wind where the gust front is located.

The clockwise veering of the environmental wind increases with height causing the mid-tropospheric wind to steer individual cells to the northeast once they form. The entire multicell system, however, moves to the east.

This type of multicell storm is often referred to as the *right-moving multicell storm*.

However, individual cell regeneration may also cause multicell storm movement to deviate substantially from the mean wind direction, resulting in different configurations of cell and storm movements and mean wind direction.

As described above, a new cell forms in or near the gust front updraft of a multicell storm, develops vertically, and moves rearward within the *front-to-rear jet*.

The new cells are generated in a discrete manner and in a remarkably periodic fashion with a period of about 10 - 15 minutes.

The cell's life cycle, which is composed of the developing stage, mature stage, and dissipating stage, as described above, occurs typically in less than an hour or so.

[Mechanisms of Cell Regeneration within a Multicell Storm:]

Based on idealized, systematic numerical experiments using nonlinear, nonhydrostatic cloud models, two major mechanisms have been proposed to explain the cell regeneration within a multicell storm:

(a) ***Advection mechanism*** (Lin et al. 1998, Lin and Joyce 2001) and

(b) ***Buoyant circulation mechanism*** (Fovell and Tan 1998).

(a) Advection Mechanism: The advection mechanism includes three stages, which are depicted in the schematic diagram of Figs. 8.6a-c.

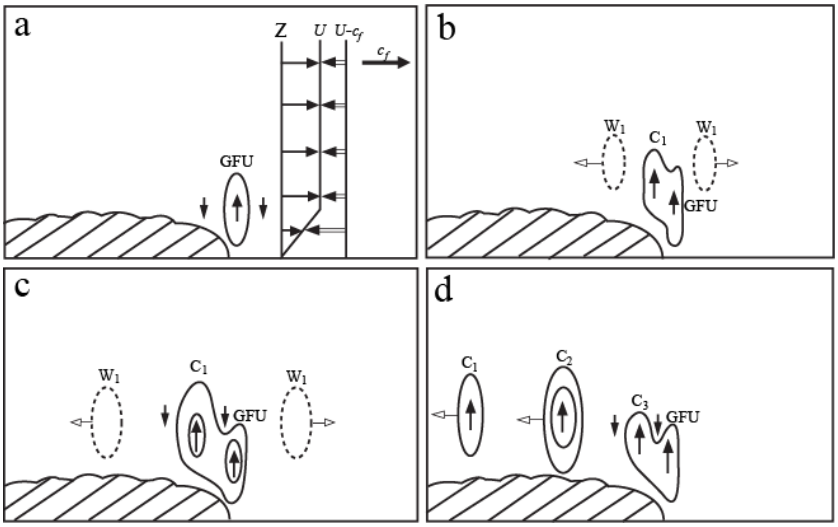

Fig. 8.6: A conceptual model of the advection mechanism for cell regeneration, development and propagation within a multicell storm in the reference frame moving with the storm (Lin et al. 1998). Three stages are found for cell regeneration: (a) Stage I: the gust front updraft (GFU) formed by low-level shear and cold outflow. Two compensating downdrafts flank the GFU; (b) Stage II: rearward advection of the upper portion of the growing GFU; and (c) Stage III: Cutting off of the growing cell (C_1) from the GFU by the upstream compensating downdraft; Panel (d) shows cell regeneration of cell C_3 and rearward movement of cells C_1 and C_2. C_2 is at the end of the growing stage (maximum vertical velocity) and C_1 is moving more quickly within the propagating stage. W_1's are the gravity waves generated by the GFU and propagate away from it. The moving speed of the gust front is denoted by c_f. (Adapted after Lin et al. 1998) [Lin 2007]

[Stage I] (Fig. 8.6a) [See Lin et al. 1998; Lin and Joyce 2001]
The gust front updraft (GFU) is forced by the cold outflow on the low-level inflow, analogous to the upward motion over the upslope of a mountain if the cold outflow is viewed as an obstacle in a moving frame of reference.

This has been shown by replacing the cold pool by a plateau in a numerical simulation of multicell storms (Fig. 7 of Fig. 7 of Lin et al. 1998; Fig. 4 of Lin and Joyce 2001).

The pressure gradient force established by the high pressure at the gust front near the ground and low pressure above the cold outflow induces the rearward and upward acceleration of the inflow, which may also contribute to the GFU formation (Parker and Johnson 2004).

The GFU may generate gravity waves that propagate away from the density current, although they may be too weak to be detected in the real atmosphere.

Two compensating downdrafts flank the GFU. An interaction between the low-level shear and the cold outflow is important and is explained by the buoyant pressure field, which will be discussed later in Section 8.3.

[Stage II] (Fig. 8.6b), as the upper portion of the GFU grows, it is advected rearward relative to the gust front, which propagates faster than the mean wind.

Relatively stronger gravity waves (W_1) are produced by this growing cell (C_1), which is still attached to the GFU.

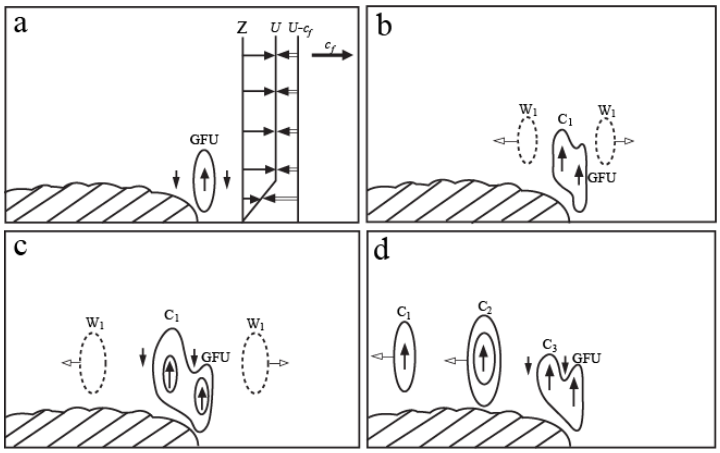

[Stage III] (Fig. 8.6c), the compensating downdrafts grow stronger as the convective cell develops further and the upstream (right) downdraft cuts off the growing cell (C_1) from the GFU.

During this stage, maximum perturbation potential temperature maxima are collocated with the updrafts in the middle and lower layers.

Stages I – III repeat and individual cells continue to be generated as the GFU keeps pushing against the mean wind.

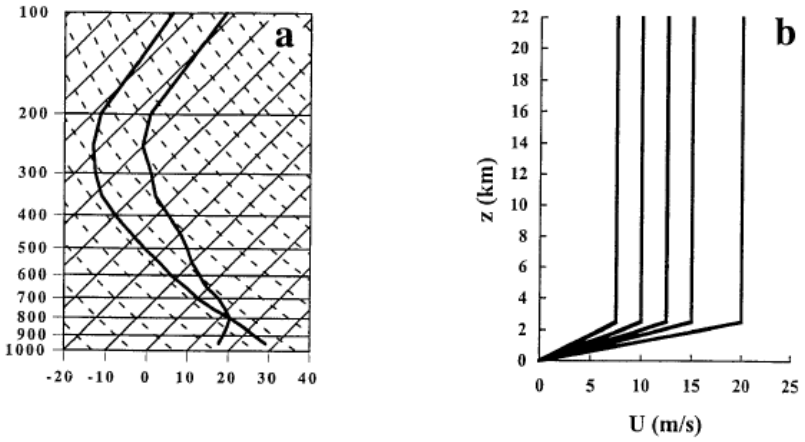

FIG. 1. (a) Skew-*T* plot of the temperature and dewpoint profiles used in the simulations. This is a smoothed version of the 1430 HNT 22 May 1976 sounding presented in Ogura and Liou (1980). (b) Wind profiles used to initialize the simulations.

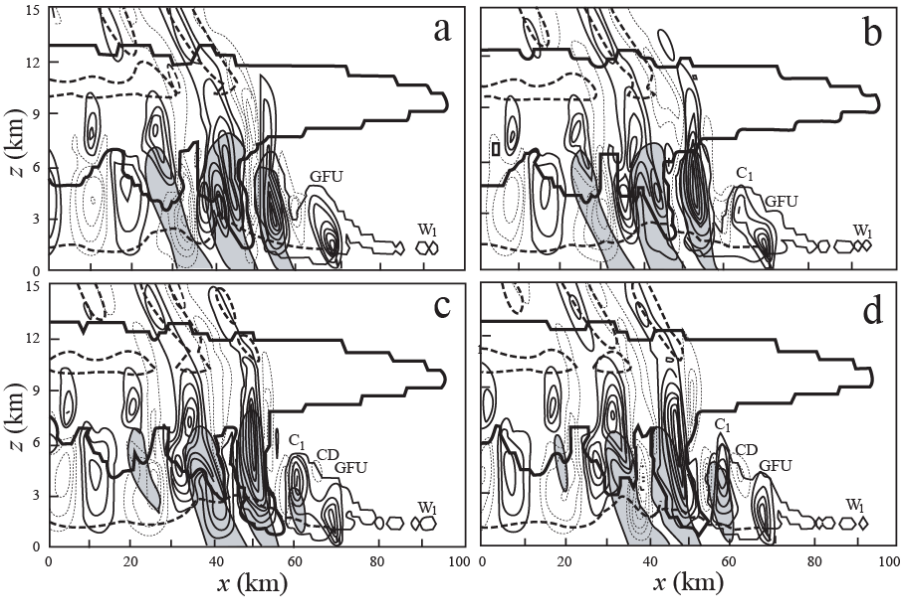

Fig. 8.7: Cell regeneration within a two-dimensional multicell storm, as simulated by a cloud model – ARPS (Xue et al. 2001). Four times the vertical velocity field in the reference frame moving with the gust front for the case with basic wind speed of U = 10 ms^{-1} above 2.5 km and linearly sheared below it are shown: (a) 252, (b) 254, (c) 256, and (d) 258 min. Positive (negative) values of vertical velocity are denoted by solid (thin dotted) contours with intervals of 1 ms^{-1}. The cloud boundary is bold contoured (> 0 g kg^{-1}). The density current is roughly represented by the -1 K potential temperature perturbation contour (bold dashed) near the surface. The rainwater is shaded (> 5 x 10^{-4} g kg^{-1}). The symbols GFU, W_1, C_1, and CD represent the gust front updraft, gravity wave 1, convective cell 1, and compensating downdraft, respectively. (Adapted after Lin et al. 1998) [Lin]

[Figure 8.7] demonstrates the advection mechanism simulated by a cloud model for cell regeneration within a two-dimensional multicell storm. At

t = 252 min (Fig. 8.7a), the GFU begins to develop vertically, signaling the generation of a new convective cell. (4/2/13)

The GFU is flanked by two downdrafts, which correspond to the stage represented in Fig. 8.6a. As the upper portion of the GFU or the new cell embryo moves rearward, compensating downdrafts begin to form on either side (Fig. 8.7b), corresponding to the stage represented in Fig. 8.6b.

The strengthening downdraft on the upstream (right) side aids in the separation of the new cell from the GFU at later times (Figs. 8.7c-d). After separation, the cell strengthens and begins to precipitate as it moves into the modified air at the rear of the system, corresponding to the stage depicted in Fig. 8.6c. Thus, the life cycle depicted in Fig. 8.4 can be explained by the advection mechanism.

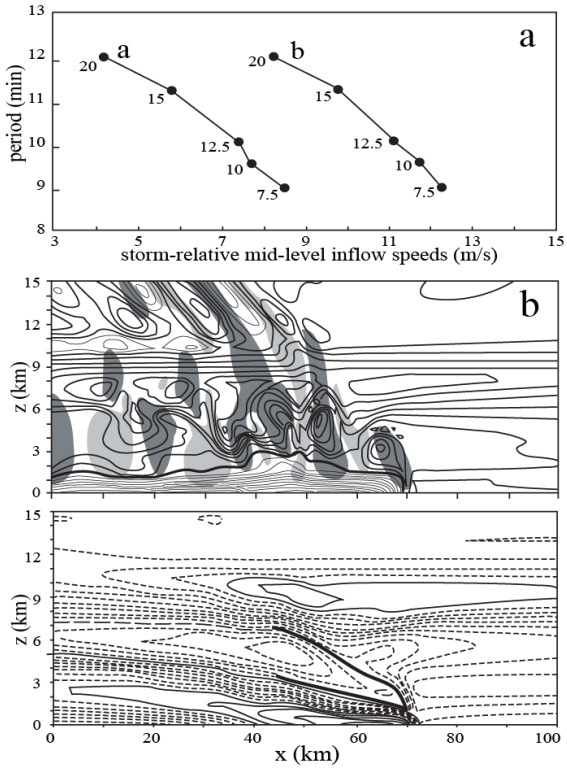

Fig. 8.8: (a) Cell regeneration period versus the far upstream storm relative midlevel inflow speeds (curve a) and the cell generation period versus the 2.5-5.5 km layer averaged storm relative midlevel inflow speeds (curve b). The numbers to the left of the curves denote the uniform basic wind speeds above 2.5 km. (b) Perturbation potential temperature fields versus vertical velocity field at t = 262 min in the moving frame with the gust front for the case of Fig. 8.7. Regions with $w > 1$ ms^{-1} are dark shaded, while regions of w < -1 ms^{-1} are light shaded. Regions of $\theta' > 0\,\mathrm{K}$ ($\theta' < 0\,\mathrm{K}$) are denoted by solid (thin solid) contours. The density current is approximately denoted by the bold contour near the surface. (c) Time-averaged,

storm-relative, total u-wind component for the case of (b). Positive (negative) values are solid (dashed) contoured with an interval of 2 ms^{-1}. Critical levels are denoted by bold curves. (Adapted after Lin et al. 1998) [Lin]

[Fig. 8.8] This numerical simulation reproduces cell regeneration and the inverse relationship between the period of cell regeneration and the mid-level, storm-relative wind speed (Fig. 8.8a).

After formation, the convective cells propagate rearward with respect to the storm movement. The cell's propagation speed increases in the trailing stratiform region.

Two distinctive modes, the *growing mode* and the *propagating mode*, can be identified for cell development and propagation, respectively.

For example, cells located in the region of 40 km < x < 70 km in Fig. 8.7 are growing with time, while those located in the region of x < 40 km are not growing, but instead are just propagating downstream.

The growing mode and propagation mode differ not only in cell growth rate and propagation speed, but also have a marked difference in their phase relationship among flow variables.

Figure 8.8b shows the phase relationship between perturbation potential temperature (θ') and vertical velocity (w') at $t = 262\,\text{min}$ for the simulated idealized multicell storm.

The basic wind, in this case, is a uniform speed of 10 ms^{-1} above z = 2.5 km and linearly decreases to 0 ms^{-1} at the surface. From Fig. 8.8b, in both the lower and middle tropospheric layers, the θ' maxima are in phase with the updrafts downstream of the gust front (40 km < x < 70 km) and are behind the updrafts farther downstream (x < 40 km).

In short, the phase relationship between θ' and w' is different in the region immediately downstream of the gust front, compared to that in the region farther downstream.

Similar to Cells n-2, n-1, n, and n+1 in Fig. 8.4 and Cells C_1, C_2, and C_3 in Fig. 8.6, the convective cells depicted in Fig. 8.8c are generated at the gust front and move downstream (in the moving frame with GFU; to the left in the figure) as they develop. These individual convective cells are at different stages of their life cycles.

[Analogy of Flow over Mountains] (see Figs. 7 and 8 of Lin et al. 1998)

- The phase relationships between the perturbation potential temperature (θ') and vertical velocity (w') as revealed in Fig. 8.8b are consistent with the numerical simulation of a squall-type multicell storm performed by Yang and Houze (1995).

- The propagating mode exhibits gravity wave characteristics. The different phase relations among flow variables between the growing mode and propagating mode can be explained by the following simple argument.

  In a quiescent, Boussinesq fluid, the thermodynamic equation, (2.2.18) reduces to

$$\frac{\partial \theta'}{\partial t} = -\frac{N^2 \theta_o}{g} w' . \qquad (8.2.1)$$

  Multiplying by θ' on both sides and taking an average over an interval of time leads to

$$\frac{1}{2}\frac{\partial \overline{\theta'^2}}{\partial t} = -\frac{N^2 \theta_o}{g} \overline{\theta' w'} . \qquad (8.2.2)$$

  For the growing mode of a convective cell,

$$\partial \overline{\theta'^2} / \partial t > 0 ,$$

  we have

$$\overline{\theta' w'} > 0$$

since $N^2 < 0$ for an unstable flow (where N is the Brunt-Vaisala frequency).

This implies that θ' is in phase with w'.

- For the propagating mode of a convective cell, θ' is out of phase with w' since $\partial \overline{\theta'^2} / \partial t = 0$. These phase relationships are depicted in Fig. 8.8b.

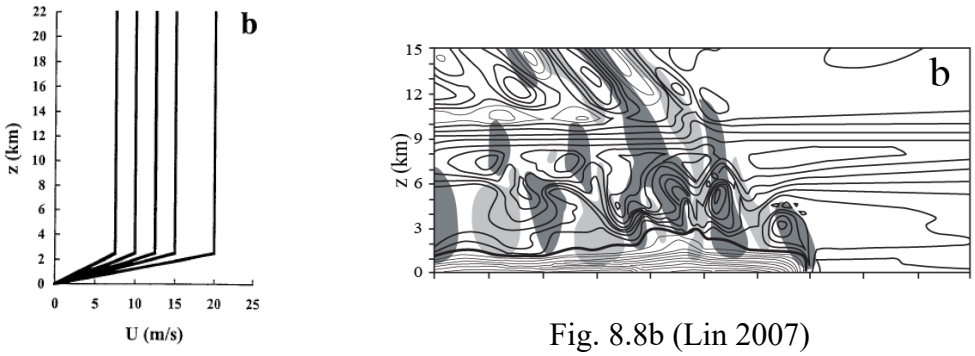

Fig. 8.8b (Lin 2007)

- The upstream phase tilt (left with hight; with respect to the basic wind and cell propagation) and phase relationships among flow variables of the disturbance (Fig. 8.8b) in the stratosphere (z > 10 km) represent an upward propagating gravity wave in a stable layer.

[Buoyant Circulation Mechanism]

- The *buoyant circulation mechanism* (summarized in Fig. 10 of Fovell and Tan 1998), however, emphasizes the importance of a local circulation induced by the heating on the strength of the forced updraft above the gust front.

- In the absence of such a local buoyancy-induced circulation, a persistent vertical updraft at the gust front would exist when a balance existed between a baroclinically generated cold pool circulation (with

negative vorticity) and a circulation associated with the low-level vertical wind shear (with positive vorticity), as proposed in the RKW theory (Rotunno et al. 1988; see subsection 8.3.1 for details).

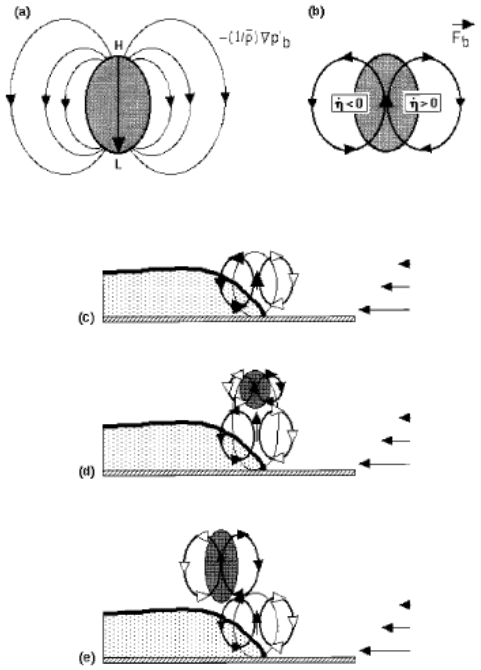

FIG. 10. Schematic illustrating the effect of an individual convective cell on the storm's low-level circulation (see text). Panel (a) shows the BPGA vector field associated with a finite, positively buoyant parcel, while (b) shows the full $\mathbf{F}_b$ field and the circulatory tendency associated with baroclinic vorticity generation $\dot{\eta}$. Panel (c) presents RKW's analysis of the circulation tendency at the subcloud cold pool (stippled region) boundary. Panel (d) adds a positively buoyant region with its attendant circulatory tendency, illustrating the initial formation of a convective cell. Panel (e) shows the cell's effect at a subsequent time.

(Fovell and Tan, 1998, MWR)

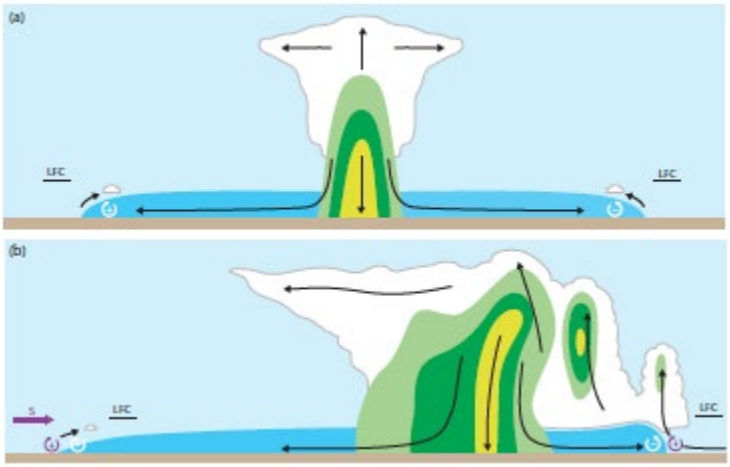

No shear

With shear

(Markowski 2010)

- Where one circulation dominates, the forced updraft tilts either upshear or downshear and is less intense. The local circulation induced by the buoyant heating in the cell developing above the gust front modulates the cold pool/shear balance, and this modulation can be divided into two phases.

- In the first phase, the horizontal part of the buoyant circulation opposes the upper part of the cold pool circulation, diminishing the effect of the cold pool to push the cell rearward. The result of this is stronger forced lifting above the gust front and so the cell grows.

- In the second phase, the cell moves rearward, as the cold pool circulation still dominates. It is as the cell moves rearward that the horizontal branch of the buoyant circulation reinforces the upper part of the cold pool circulation, driving air parcels rearward and leading to weaker forced lifting.

  As the cell moves further rearward, the effect of the buoyant circulation on the cold pool/shear balance at the gust front diminishes, the forced updraft intensifies again, and the process repeats. A primary difference between the advection mechanism and this buoyant circulation mechanism is the importance of the compensating subsidence in the former and the modulation of the cold pool/shear balance in the latter.

11.3 Effects of shear and buoyancy

11.3.1 Effects of shear on cold outflow

- Observations indicate that ambient wind and precipitation play important roles in the dynamics of severe convective storms.

  The ambient wind, and in particular the vertical wind shear, may affect the organization, development, and propagation of a severe convective storm.

  The precipitation associated with a severe convective storm may produce a density current via evaporative cooling, which in turn may affect the strength and propagation of the gust front, eventually influencing a new storm's development and propagation.

- Another factor which affects precipitation directly is the buoyancy of the environmental air.

  In a conditionally unstable atmosphere, the buoyancy can be measured by the CAPE, which is required for storms to develop.

  Observations of convective storms indicate that vertical wind shear increases for each ascending level of storm type:

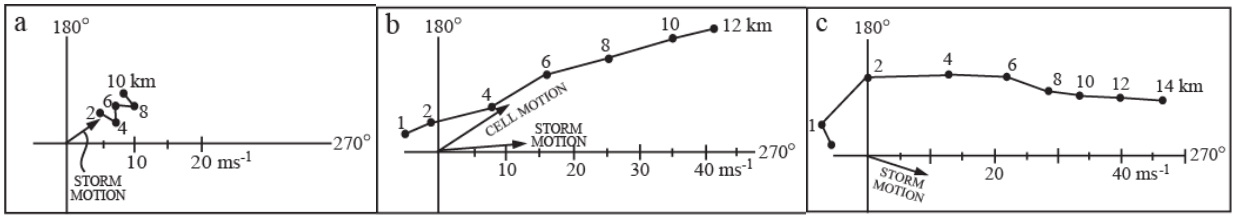

(a) single-cell (b) multicell (c) supercell

(Lin 2007)

- Effects of environmental shear on severe convective storms and mesoscale convective systems have long been recognized by observations from upper-air soundings.

- The most severe and long-lasting storms typically form in strongly sheared environments.

  Severe convective storms often occur in the vicinity of upper-level polar jets and/or subtropical jets, and low-level jets (e.g. Fig. 8.10), which may entail the vertical wind shear in the synoptic environment.

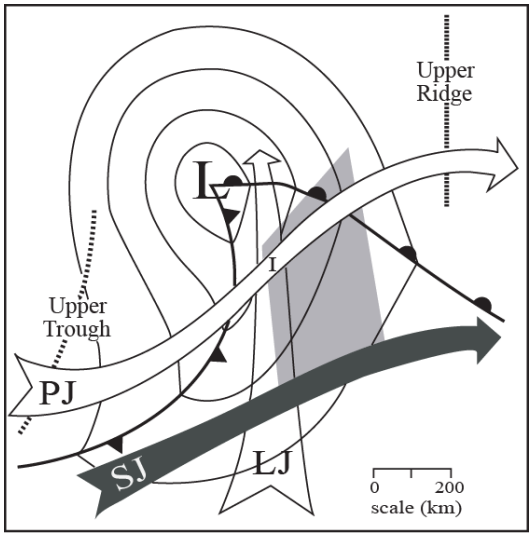

Fig. 8.10: A schematic of the synoptic environment conducive to severe convective storm outbreaks. Symbols are denoted as follows: LJ: low-level jet; PJ: polar jet; SJ: subtropical jet; I: intersection of PJ and LJ; and light-shaded area: area of severe convection. Surface features are denoted by conventional symbols. (After Barnes and Newton 1986)

- In addition, it has been proposed that vertical wind shear plays an important role in maintaining squall lines.

- For a better understanding of the basic dynamics of squall lines, we will first discuss the shear effects on convective lines in a two-dimensional framework.

  The longevity of a two-dimensional squall line may be discerned through the schematic depicted in Fig. 8.11.

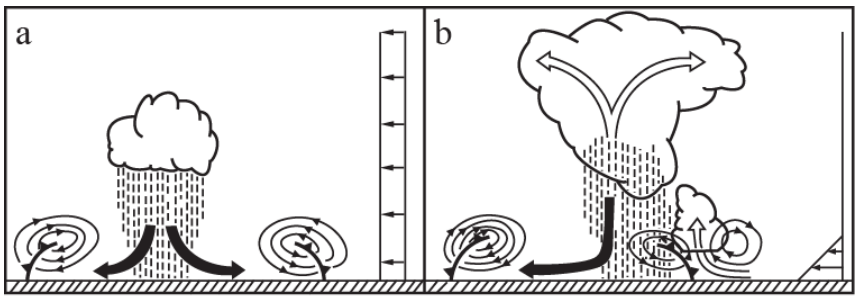

Fig. 8.11: Schematic diagram for convective cell development in an environment without shear (a) and with low-level shear (b). In (b), the presence of low-level shear allows the shear-induced circulation to balance the cold-outflow induced circulation and produce deeper lifting on the downshear side. Note that downshear means the downstream side of the shear vector or the right -and side in the case of panel b. This is known as the RKW (Rotunno, Klemp, and Weisman 1988) theory.

- A two-dimensional convective cell in an environment with no vertical shear would, via evaporative cooling, produce a pair of surface outflows that move rapidly away from the convective cell. The convective cell would dissipate quickly in a way similar to the ordinary single cell shown in Fig. 8.1.

- If the low-level shear exists in the ambient wind, it may prevent the cold pool from developing into a density current that moves away from the convective cell, and support the original cell to develop into deep convection (Thorpe et al. 1982).

- Based on a vorticity argument (Rotunno et al. 1988), in the absence of low-level shear (Fig. 8.11a), the circulation of a spreading cold pool would inhibit deep lifting, which would prevent the triggering of a convective cell.

  On the other hand, the presence of low-level shear (Fig. 8.11b) would allow the shear-induced circulation to counteract the cold-outflow induced circulation.

When these circulations are in balance, i.e. the *optimal state*, a deeper lifting is produced on the downshear side of the cold pool.

The long-lived state is characterized not by a long-lived cell, but by a long-lived system of convective cells, such as the multicell discussed earlier, that are constantly generated at the gust front on the downshear side. This mechanism is referred to as the RKW theory for squall lines.

- The RKW theory addresses the question of how the shear influences the transformation of ordinary thunderstorms into a long-lasting convective system where cells are continuously generated along a line.

  This theory identifies three stages in the evolution of a convective system (Fig. 8.12). The vorticity dynamics of each stage can be deduced from the y component of the vorticity (η) in a two-dimensional Boussinesq fluid flow (homework)

$$\frac{D\eta}{Dt} = -\frac{\partial b}{\partial x}, \qquad (8.3.1)$$

(*The original (8.3.1) of Lin 2007 is simplified here.)
where

$$\eta = \frac{\partial u}{\partial z} - \frac{\partial w}{\partial x}, \qquad (8.3.2)$$

and b the buoyancy, u the cross-convective line velocity, and w the vertical velocity.

[Early Stage] No significant cold pool is yet produced and the stage is characterized by $c << \Delta U$.

Air parcels ascend from the boundary layer and have an initial positive vorticity, $\eta_i = dU(z)/dz$.

Because there is little or no outflow, there is no low-level baroclinic modification of η . Therefore, at higher levels, a net positive bias prevails, causing the axis of the updraft to tilt in the downshear direction (Weisman and Rotunno 2004).

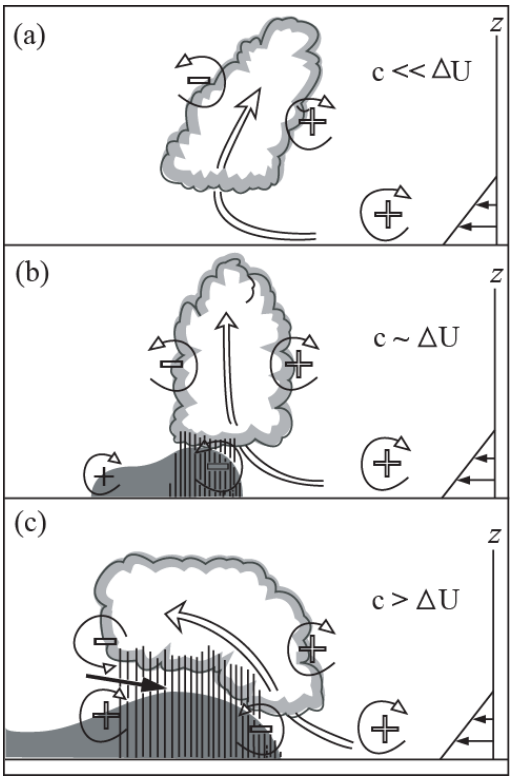

Fig. 8.12: Three stages in the evolution of a convective system, based on the RKW theory (Rotunno et al. 1988). (a) When $c << \Delta U$, the updraft tilts downshear (to the right) with height. (b) When $c \approx \Delta U$, the updraft becomes upright due to the balance between the ambient shear and the circulation induced by the cold pool. (c) When $c > \Delta U$, the updraft tilts upshear. Symbols c and ΔU represent the speed of the density current generated by the cold pool and the ambient low-level vertical wind shear, respectively. The updraft current is denoted by the thick, double-lined flow vector, and the rear-inflow in (c) is denoted by the thick solid wind vector. The surface cold pool is shaded and areas of rainfalls are depicted by vertical lines. Regions of significant horizontal vorticity are denoted by thin, circular arrows. Clouds are outlined by thick grey curves. (Adapted after Weisman 1992) [Lin 2007]

[Second Stage] A cold pool is produced from evaporative cooling associated with the rainfall (Fig. 8.12b).

The system then evolves to a state where $c \approx \Delta U$.

The cold pool generates an additional negative η of comparable strength to the positive η at the downshear (right) side of the cold pool.

The generation of this additional negative vorticity helps make the main updraft of the convective system upright.

[Final Stage]

The cold pool continues to intensify.

The system evolves to the state for $c > \Delta U$ (Fig. 8.12c).

New cells are generated continuously at the gust front of the downshear (right) propagating outflow boundary.

On the upshear side, the surface cold pool and heating aloft baroclinically generate a rear-inflow jet. The system tilts upshear at this stage.

Most squall lines tend to evolve through all three stages.

- Rotunno et al. (1988) claim that the second stage, where $c/\Delta U \approx 1$, represents an *optimal state* for convective system development.

  At this optimal state, the system that maintains an upright configuration and the deepest lifting is produced at the leading edge of the cold pool. This helps explain the observed longevity of some squall lines, although it does not exclude the fact that squall lines can be long-lived even when they are not in an optimal state.

- It can be derived that for a steady balanced state, the speed for a two-dimensional density current generated by a square cold pool with a finite volume is (Rotunno et al. 1988)

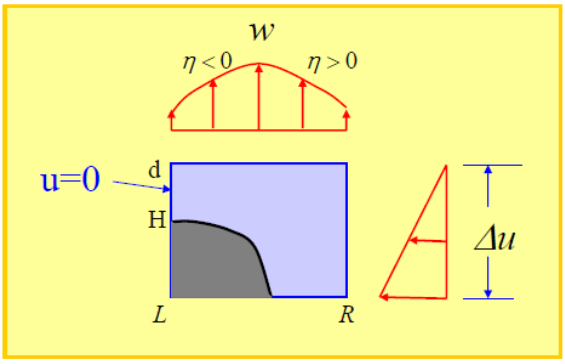

$$c = \sqrt{-2bH} = \Delta U\,, \qquad (8.3.3)$$

where H is the height of the density current and b is the buoyancy

$$b = \frac{g\Delta\theta}{\theta_o}\,. \qquad (8.3.4)$$

In (8.3.4), $\Delta\theta$ is the potential temperature deficit of the cold pool from its environment. The density current speed estimated by (8.3.3) is identical to that estimated by Benjamin (1968).

- The above vorticity argument for shear and cold pool interaction can be illustrated through a series of idealized numerical experiments for a dry, unstratified flow with low-level shear passing over a cold pool of air in the two-dimensional volume of $|x| \le 1$ and $0 \le z \le 1$.

  A two-dimensional vorticity-streamfunction model may be constructed to solve the following governing equations in the x-z plane (adding friction to Eq. (8.3.1); Weisman and Rotunno 2004):

$$\frac{D\eta}{Dt} = -\frac{\partial b}{\partial x} + \nu\nabla^2\eta\,, \qquad (8.3.5)$$

$$\frac{Db}{Dt} = \nu \nabla^2 b \,, \tag{8.3.6}$$

$$\nabla^2 \psi = \eta \,, \tag{8.3.7}$$

where $D/Dt \equiv \partial/\partial t + u\partial/\partial x + w\partial/\partial z$, b is the buoyancy, ψ the streamfunction, and ν the kinematic viscosity and the streamfunction is defined by

$$u = \partial\psi/\partial z \text{ and } w = -\partial\psi/\partial x \,.$$

All the variables associated with this model and in relevant results are nondimensionalized.

- Figures 8.13a-c illustrate the impacts of the interaction between low-level shear and the cold pool on the flow after a nondimensional simulation time $t = 4$.

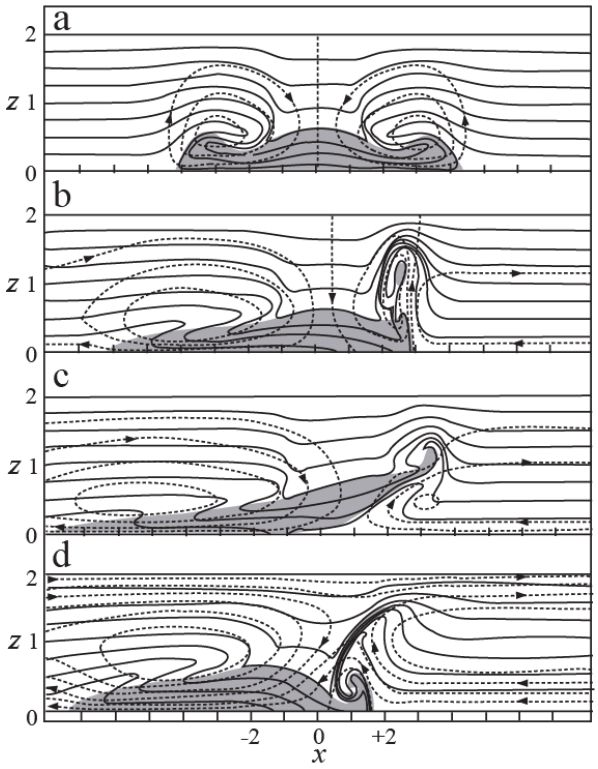

Fig. 8.13: Effects of the interaction between the vertical wind shear and cold pool on the flow circulation and density current, as illustrated through a series of idealized numerical experiments

for a dry, unstratified flow with low-level shear passing over a prescribed cold pool of air in the box of $|x| \le 1$ and $0 \le z \le 1$ after a nondimensional time $t = 4$. The basic flow is assumed to be 0 at the surface, increasing to: (a) $\Delta U = 0$, (b) 0.85, and (c) 1.5 at $z = 0.5$, and remains constant above $z = 0.5$. In (d), a deep shear is used. The basic flow speed increases linearly from 0 at the surface to $\Delta U = 2.0$ at $z = 2$. Areas with buoyancy $b < -0.5$ are shaded; the streamfunction ψ is denoted with dashed lines; and the tracer fields are denoted by heavy solid lines. (Adapted after Weisman and Rotunno 2004)

- The nondimensional time may be defined as $t = \tilde{U}\tilde{t} / \tilde{a}$, where $\tilde{U}$ is the dimensional average wind speed in the shear layer (= $\Delta\tilde{U}/2$), $\tilde{t}$ the dimensional time, and $\tilde{a}$ the dimensional half-width of the initial cool pool.

- For $\tilde{U} = 10$ ms^{-1} and $\tilde{a} = 10$ km, a nondimensional time of t = 4 corresponds to 4000 s. At this time, the basic flow is assumed to be 0 at the surface, increasing to $\Delta U = 0$, 0.85, and 1.5 at $z = 0.5$, and remaining constant above $z = 0.5$.

- In the case of no vertical shear (Fig. 8.13a), the cold pool initially spreads in both $+x$ and $-x$ directions, but eventually spreads to the whole domain in the absence of ambient shear.

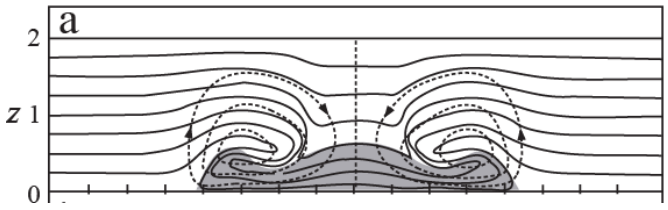

- In the case of $\Delta U = 0.85$, the cold pool tilts downshear initially due to the presence of +y-vorticity generated vertical shear.

However, by $t = 4$ (Fig. 8.13b), this tendency is balanced by the cold-pool generated $-y$-vorticity on the downshear (right side in the figure) edge, which results in deep lifting.

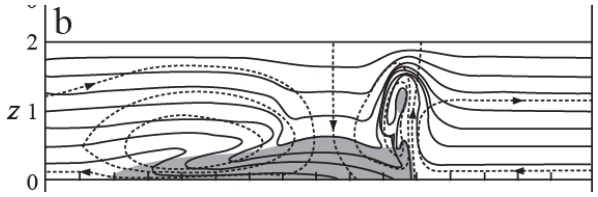

This is the *optimal state* according to the RKW theory.

- When the shear increases to $\Delta U = 1.50$ (Fig. 8.13c), the vorticity generated by the vertical shear becomes too strong, upsetting the balance with the cold-pool generated vorticity.

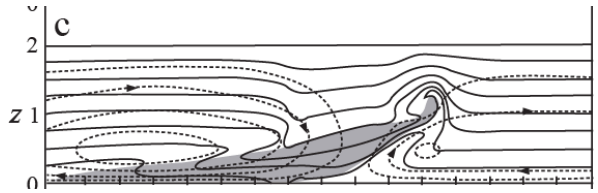

This imbalance causes the circulation to tilt downshear, resulting in a more shallow lifting than in the case of $\Delta U = 0.85$.

- When the depth of the shear layer increases to the entire domain, $z = 2$ (Fig. 8.13d), the lifting is weaker but otherwise similar to that in the optimal state (Fig. 8.13b).

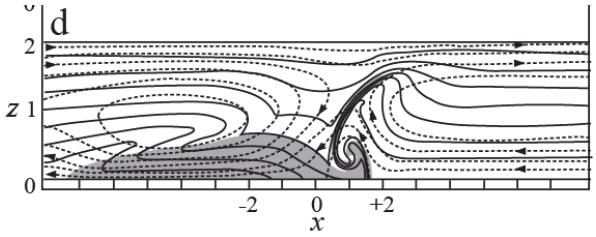

- Application of the RKW theory to squall-line dynamics will be discussed in the next chapter.

11.3.2 Effects of buoyancy

- In addition to the vertical wind shear, storm development may also be influenced by buoyancy.

  When the available buoyancy increases, the intensity of induced convection tends to strengthen.

  This, in turn, will produce heavier rainfall and increase evaporative cooling, thereby strengthening the surface outflow.

  Strengthening the surface outflow or density current tends to increase the propagation speed of the gust front.

- As defined in (7.3.2), the buoyancy will contribute to vertical acceleration or deceleration.

  Because CAPE is an integrated quantity of parcel buoyancy, it may serve as a measure of the effect of buoyancy.

  It can be approximated to that the theoretical maximum speed of an updraft is $w_{max} = (2\text{CAPE})^{1/2}$, based on the assumption that all the CAPE is converted into the air parcel's kinetic energy.

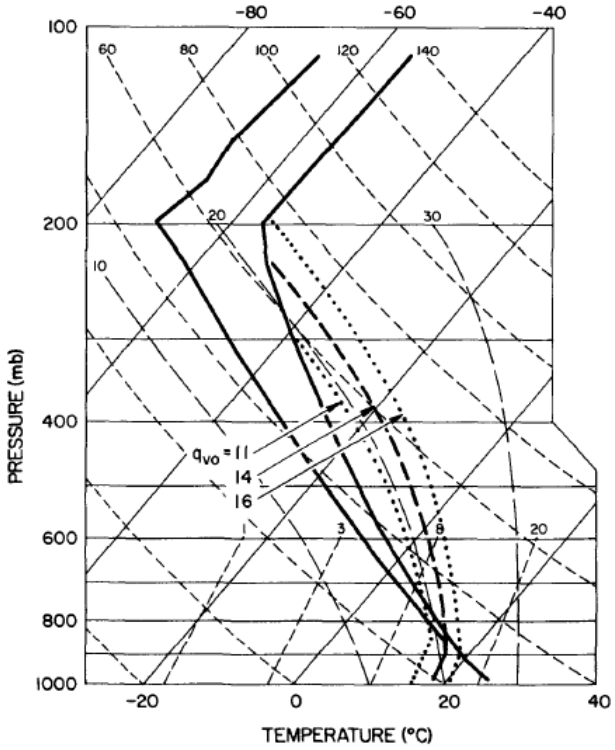

FIG. 1. Skew T diagram depicting temperature and moisture profiles used in model experiments (heavy solid lines). Heavy dashed line represents a parcel ascent from the surface based on a surface mixing ratio q_{vo} = 14 g kg^{-1}. Heavy dotted lines represent similar parcel ascents for q_{vo} = 11 g kg^{-1} and 16 g kg^{-1}. Tilted solid lines are isotherms, short dashed lines are dry adiabats, and long dashed lines are moist adiabats.

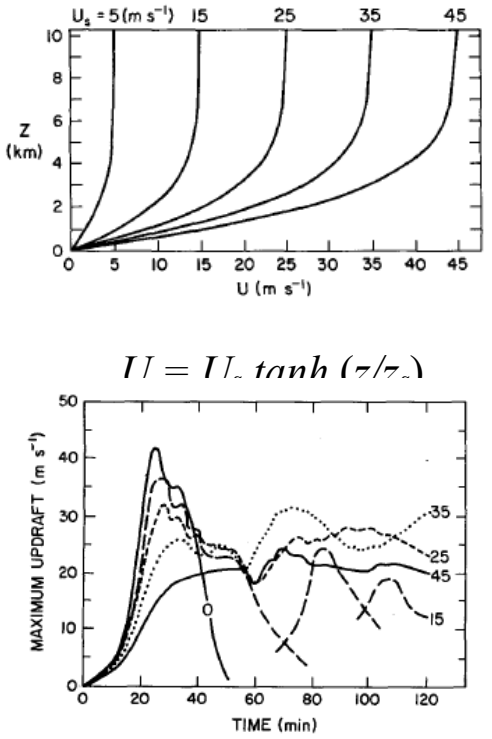

FIG. 3. Time series of maximum vertical velocities for the U_S = 0, 15, 25, 35 and 45 m s^{-1} wind shear experiments. q_{vo} = 14 g kg^{-1}.

(Weisman and Klemp 1982, MWR)

- Three examples, based on idealized numerical simulations, are given in Fig. 8.14, in which $q_{vo} = 11$, 14 and 16 g kg^{-1} corresponds to CAPE = 1000, 2200, and 3500 m^{2}s^{-2}, respectively.

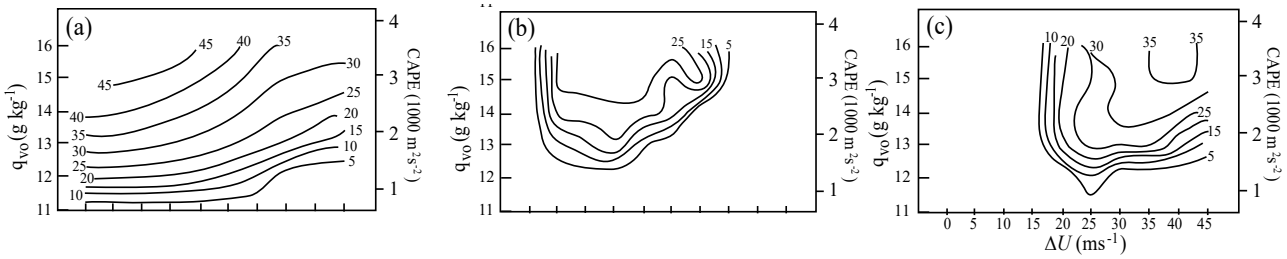

Fig. 8.14: Effects of the vertical shear (ΔU) and CAPE on storm development in idealized numerical experiments. The basic wind ($U(z)$) follows (8.4.1) with $z_o = 3$ km. The maximum vertical velocity (ms^{-1}) in the domain for (a) initial storms (in the first 30 min), (b) secondary (redeveloped) storms and (c) split storms is plotted on the parameter space (ΔU, CAPE). The $w_{\max}$ for (a) is obtained in the initial updraft which occurs approximately 30 min into the simulation. In these simulations, CAPE has been altered by varying the surface water vapor mixing ratio. (Adapted after Weisman and Klemp 1982) [Lin 2007]

- These examples demonstrate that the environmental vertical shear and buoyancy play essential roles in determining the storm types, such as a short-lived ordinary single cell storm, a multicell storm or a supercell storm.

- As discussed Section 8.2, the advection effect may cause the max *w* of the initial updraft to decrease as the low-level vertical shear increases.

- When shear strength is kept constant and CAPE increases, the maximum vertical velocity of the initial storm increases (Fig. 8.14a). The threshold CAPE required to sustain moist convection for the given initial impulse is about 1000 m^2s^{-2}.

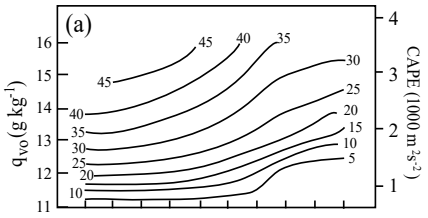

Fig. 8.4 (Lin 2007)

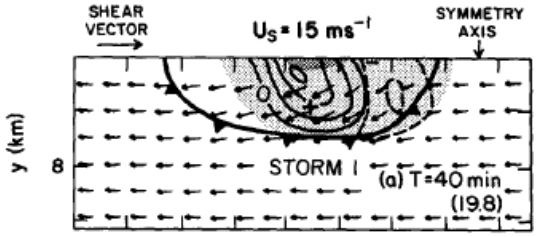

x (km)

- As shown in Fig. 8.14b, the development of the secondary storm occurs when the environment has high CAPE and low-to-moderate shear. A second storm will not develop if no shear exists.

  This effect may be explained by the RKW theory: the balance between the storm relative inflow, which is controlled by the low-level shear (ΔU), and storm-induced surface outflow, which is controlled by the CAPE, prevents the development of a secondary storm.

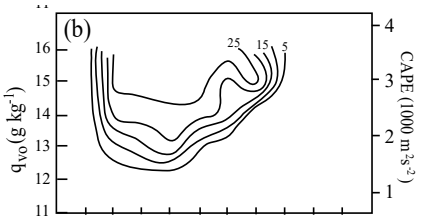

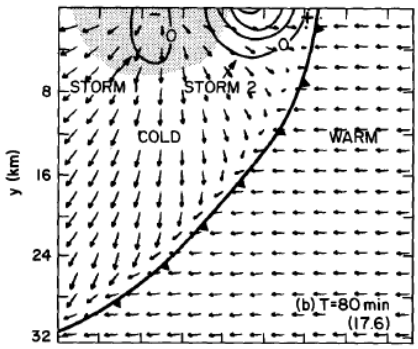

- The supercell regime, which induces storm splitting, exists at only moderate to high shear flows (Fig. 8.14c). The optimal development of a supercell storm, i.e. the maximum intensities of a split storm, is reached when both CAPE and low-level shear increase.

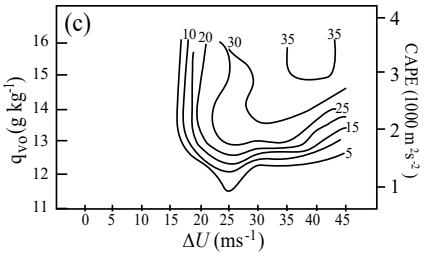

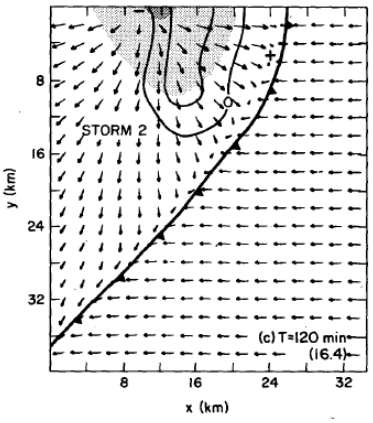

➢ Based on the above discussions, the dependence of the simulated storm types on environmental buoyancy and low-level shear may be consolidated and generalized in terms of a nondimensional control parameter, namely the *bulk Richardson number*,

$$R_B \equiv \frac{CAPE}{(\Delta U)^2/2}, \tag{8.3.8}$$

where ΔU is the difference between the mid-level (e.g., 6 km) density-weighted mean wind speed and the mean near surface layer (e.g., 500 m) wind speed.

For a directional shear, the denominator of (8.3.8) is replaced with $[(\Delta U)^2 + (\Delta V)^2]/2$.

The numerator is a measure of potential updraft strength but is also indirectly a measure of potential downdraft and surface outflow strength. The denominator may be interpreted as a measure of the inflow kinetic energy made available to the storm by the vertical wind shear.

Operationally, R_B is less used; instead, the CAPE and shear are used separately to help make predictions of the occurrence of severe storms.

Based on idealized numerical experiments, the nondimensional storm strength may be defined as

$$S = \frac{w_{\max}}{\sqrt{2CAPE}}, \tag{8.3.9}$$

and can be displayed as a function of the bulk Richardson number (Fig. 8.15).

- Note that $w_{\max}$ is the model simulated maximum vertical velocity within the domain, and the denominator is the theoretical $w_{\max}$ for a certain *CAPE* (Ch. 7, Lin 2007).

  However, the air parcel may not normally attain this value in the real atmosphere due to some assumptions made in the parcel theory, such as neglecting mixing and entrainment, and the immediate adjustment of the air parcel pressure to its environmental pressure.

- The initial storm strength S increases as R_B increases (Fig. 8.15a). Updrafts cease to develop into storms for small R_B, such as $R_B <$ 10, under the same initial forcing. This may be explained by the RKW theory by assuming that the strength of the cold pool is proportional to CAPE.

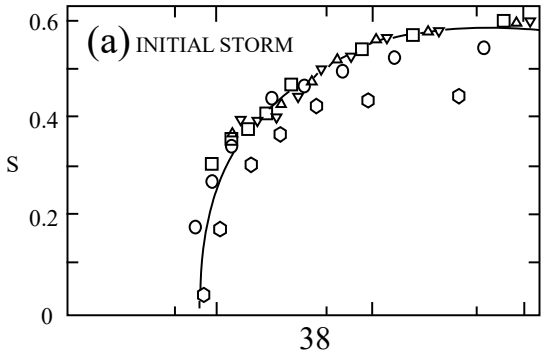

Fig. 8.15: [abscissa is R_B] Simulated storm strength S, defined in (8.3.9), versus the bulk Richardson number R_B for (a) initial storms, (b) secondary storms, and (c) split storms. (After Weisman and Klemp 1982)

- Thus, for a fixed CAPE, small R_B implies that shear is too strong for $C << \Delta U$ to be balanced by the cold pool (C). Figure 8.15b shows the multicell storm strength S as a function of R_B for the secondary storm. No secondary storm development occurs for $R_B <$ 35.

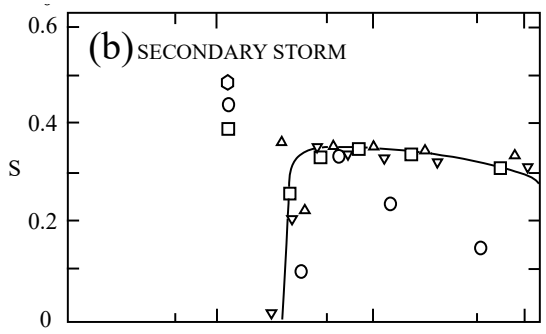

Fig. 8.15 (Lin 2007)

- The values of R_B for supercell storm development are concentrated in the range of $15<R_B<35$, based on the numerical simulations shown in Fig. 8.15c. For $R_B < 10$, the shear is too strong to allow for storm growth, while for $R_B > 50$, strong buoyancy produces a density current that is too strong for the shear to balance.

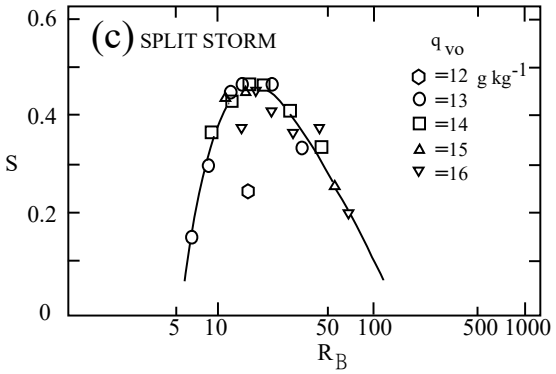

- These results suggest that unsteady, multicellular convection occurs for $R_B > 35$ and that supercell convection occurs when $10 < R_B < 50$.

  Note that the critical values of R_B for different storm regimes are model-dependent, where a model's output may be affected by numerical schemes used, such as microphysics parameterization schemes and numerical diffusion.

  For example, the model used for generating results shown in Fig. 8.15 is very diffusive. The numerical diffusivity may smooth out disturbances. Thus, the critical R_B values, such as 10, 35, and 50, discussed above should be used for reference only.

- Several limitations are encountered in representing storm characteristics with one or two nondimensional control parameters, such as the bulk Richardson number (R_B) and nondimensional storm strength (S) in the above experiments.

  R_B represents the ratio of PE to KE or indirectly represents the force balance created between the U_z and surface cold outflow.

  The CAPE in S indirectly represents the strength of the surface cold outflow or density current.

  However, the strength of the surface cold outflow may also be influenced by other factors, such as vertical distribution of moisture content and detailed microphysical processes.

- In fact, the strength of the surface cold outflow is arguably more directly related to a parameter called the *downdraft convective available potential energy* (DCAPE), than the CAPE.

  Similar to (7.3.29), DCAPE may also be defined as

$$DCAPE = g \int_{z_S}^{z_i} \frac{\bar{\theta}(z) - \theta(z)}{\bar{\theta}(z)} dz \,. \qquad (8.3.10)$$

DCAPE is physically equivalent to the kinetic energy gained by a parcel descent from a certain height (z_i) to the surface.

The parcel temperature is obtained by cooling it to saturation via the wet-bulb process and then lowering the parcel saturated- or pseudo-adiabatically with just enough evaporation to keep it saturated.

When rain evaporates in subsaturated air or solid precipitation (snow or hail) melts at the melting level or sublimates, the cooled air generates a downdraft. Thus, the maximum downdraft may be estimated by $-w_{\max} = \sqrt{2DCAPE}$.

Idealized numerical simulations indicate that storm development is also controlled by *DCAPE* and the mid-tropospheric moisture content (dryness) (e.g., Gilmore and Wicker 1998).

Although DCAPE may more accurately measure the strength of the surface cold outflow, it does not address how much precipitation will be produced.

Thus, finding a small set of control parameters for representing storm characteristics continues to be a challenging task.

11.4 Dynamics of supercell storms

11.4.1 General characteristics

- A *supercell* storm is defined as a convective storm that possesses a persistent, deep, rotating updraft.

  These rotating updrafts are often found in conjunction with mesocyclones.

  A *mesocyclone* is a cyclonically rotating vortex, around 2 to 10 km in diameter, that has a vorticity on the order of 10^{-2} s^{-1} or greater.

  Most supercell storms are characterized by the following features:

  - They are situated in an environment with strong vertical wind shear.
  - A mesocyclone, with a diameter of several kilometers, associated with a rotating updraft is often embedded in a supercell storm.
  - They often propagate in a direction dictated by the mean environmental wind.
  - They tend to last for several hours due to strong vertical shear in their environment.
  - Although some supercell storms have a size comparable to that of multicell storms, their cloud structure, flow circulation, and formation processes of precipitation are organized by a single massive updraft-downdraft pair.
  - Sometimes a pair of supercells are produced through a splitting process with a cyclonic supercell moving toward the right (with respect to the mean wind), and an anticyclonic supercell moving toward the left.

- The rightward propagation of a supercell storm is related to the veering of the environmental wind shear vector.
- Most precipitation falls downshear from the main storm updraft, which lies above the intersection of the forward and rear flank gust fronts.
- Supercell storms tend to produce the most intense, long-lasting tornadoes and damaging hail through complicated processes.
- Tornadoes may develop in regions where the environmental inflow and storm outflow meet beneath the mesocyclone or along the nose of the gust front.
- A supercell usually has a very organized internal structure that enables it to propagate continuously.

➢ Figure 8.16 shows the schematics of vertical and horizontal structures of a mature supercell storm observed by radar in northeast Colorado.

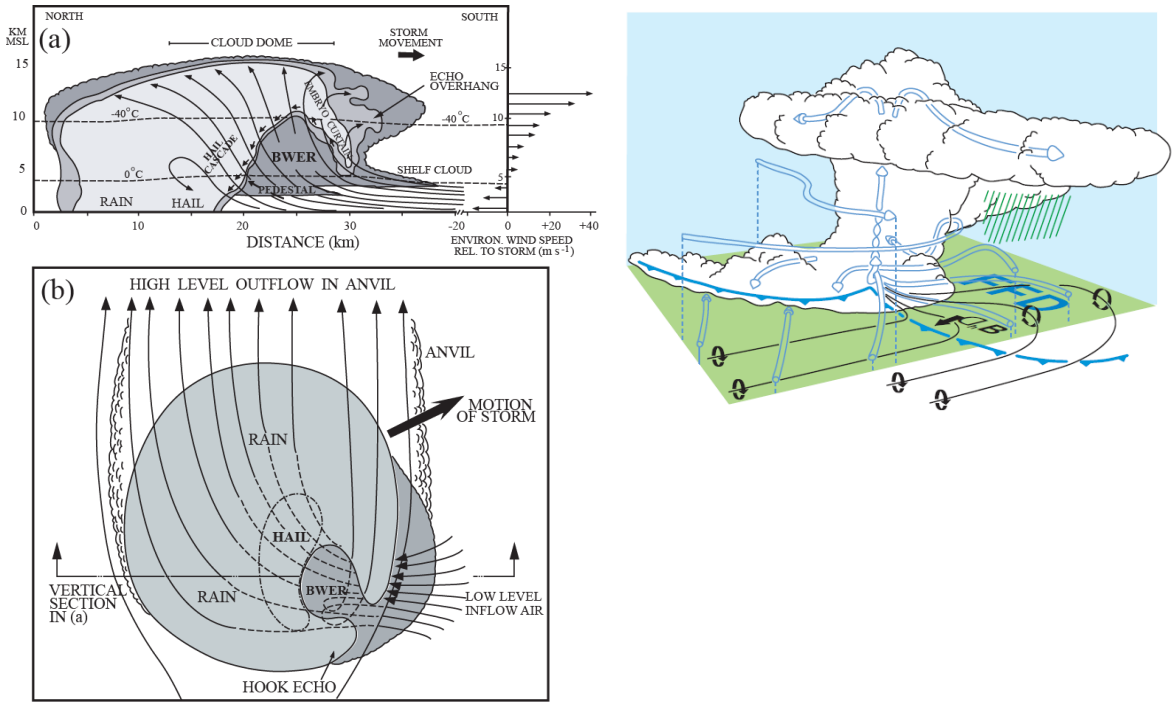

Fig. 8.16: Vertical and horizontal structure of a mature supercell storm. (a) The vertical cross section is taken along the direction of storm movement through the center of the main updraft. The shaded regions represent two levels of radar reflectivity. Areas of weak echo region or bounded weak echo region (BWER) are shaded. Arrows to the right of the figure indicate the environmental wind relative to the storm movement. Arrows within the figure denote projections of streamlines of airflow relative to the storm movement. (b) The horizontal view at the height of 5.2 km of (a) seen from above. The major region of radar reflectivity in (b) is light shaded. (Adapted after Browning and Foote 1976) [Lin 2007]

- This cross section is taken along the direction of storm movement through the center of the main updraft. The supercell's massive updraft (Fig. 8.16a) is very intense (~10 – 40 ms^{-1}), and significantly larger than that of a single-cell storm or multicell storm (Fig. 8.4).
- The cloud droplets within the updraft are swept upward to a level of about -40°C and may penetrate to tropopause. Since the cloud droplets within this intense updraft have insufficient time to grow, they cannot produce strong radar echoes.
- Instead, they form a *hook echo* (as seen in radar images) that wraps around a so-called *weak echo region* (WER) or *bounded weak echo region* (BWER), often located along the right flank, facing the direction of the storm movement (Fig. 8.16b).
- The largest amount of hail falls to the ground in a narrow band behind the BWER, while rain falls on the ground in a wider region behind the region of hail. An *echo overhang* can be found on the forward flank of the supercell storm.
- A *hook echo* wraps around the BWER at the midtroposphere horizontal plane.
- The hook's cyclonic shape results from the mesocyclone's cyclonic winds. The hook itself is actually a result of the mesocyclone, a region of rotation with cyclonic vortex and rising air.
- Many of the violent tornadoes associated with supercells exhibit a distinct hook echo in radar images. To a weather forecaster, a hook echo is one clue that a supercell has the potential to produce a tornado.

- Figure 8.17 shows a hook echo in a radar image taken at 2356 UTC 3 May 1999 from the Oklahoma City's Doppler radar.

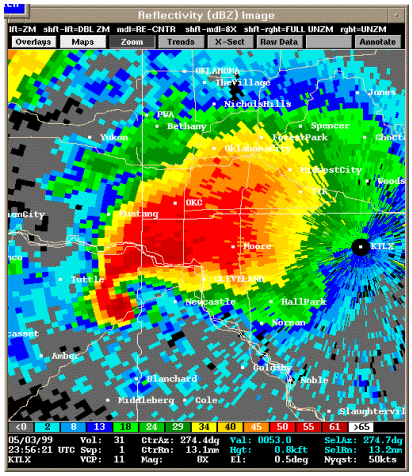

Fig. 8.17: A hook echo shown in a radar image taken at 2356 UTC 3 May 1999 from KTLX, the Oklahoma City WSR-88D. The storm produced a 1/4 to 1/2 mile wide F5 tornado in the Oklahoma community of Bridge Creek shortly after the image was taken. (Courtesy of NWS Norman, Oklahoma. Image was provided by C. J. Ringley)

  - The storm was responsible for a 1/4 to 1/2 mile wide tornado that was rated F5 on the Fujita Scale of tornado intensity in Bridge Creek, Moore, and Oklahoma City, Oklahoma after the image was taken.

- Note that many supercells have hook echoes, but only a small fraction produce tornadoes.

  While there are many factors that signal the formation of a tornado, the hook echo is the only one that can be captured by conventional radar.

  However, it has also been found that Doppler velocities serve as a significantly better indicator of tornadoes than the hook echo.

- A typical supercell storm evolves through three stages: (a) initial stage, (b) developing stage, and (c) mature stage.

    - At the initial stage, the supercell storm is no different from that of a single convective cell in an ordinary single-cell storm or embedded in a multicell storm.

      At this stage, the storm moves in the mean wind direction and no weak echo regions (WERs) or overhang echoes are present.

      A WER develops in the region of strengthening updraft. Approximately 90 minutes into the storm lifetime, the supercell reaches its quasi-steady mature stage.

      At this stage, a BWER develops from the WER, which coincides with the strong updraft. A BWER is usually associated with a strong updraft.

      The basic structure of a supercell includes several important features such as a shelf cloud, wall cloud, tornado, tail cloud, hail and rain locations, virga, anvils, mammatus cloud, and penetrating cloud top.

      In addition, during tornadogenesis, particular flow features such as the *forward flank downdraft* (FFD) and *rear flank downdraft* (RFD) may form within a supercell storm (Fig. 8.26).

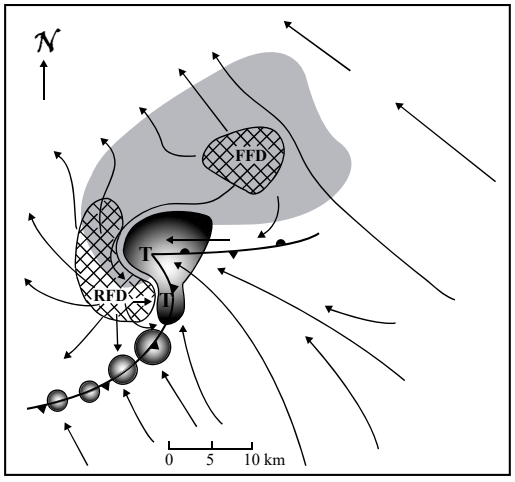

Major features associated with this type of supercell storm have been reasonably well-simulated by nonlinear, nonhydrostatic cloud models.

- Supercell storms may be classified as: (a) *classic supercell*, (b) *high precipitation* (HP) *supercell*, and (c) *low-precipitation* (LP) *supercell*.

- In a classic supercell, most of the precipitation falls downwind from the main storm updraft. The updraft lies above the interaction of the forward flank and rear flank gust fronts.

  Tornadoes usually develop in regions where the environmental inflow and storm outflow meet beneath the mesocyclone or along the nose of the gust front.

  When there is a balance between low-level outflow and inflow, long-lived or multiple tornadoes tend to occur because the mesocyclone does not occlude rapidly (Wakimoto et al. 1996).

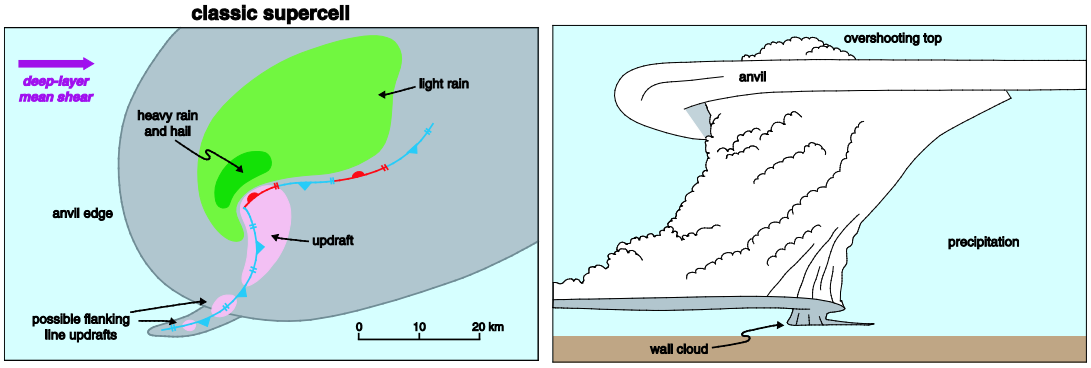

(Markowski & Richardson 2010)

- HP supercells occur less frequently in the High Plains of the USA, but are predominant elsewhere, such as Ohio Valley, Gulf Coast and Southeastern USA.

  The HP supercell exhibits the following characteristics:
  - It tends to be larger than the classic supercell.
  - The mesocyclone and tornadoes created by the storm are largely embedded in precipitation.
  - It exhibits a distinctively kidney or S-shaped echo patterns, inflow notches, and persistent weak-echo regions.
  - It may contain multiple reflectivity cores.
  - Hook echoes, if present, are often very broad.
  - Many HP supercell storms undergo a life cycle in which they evolve from one form to another, transitioning from classic to high-precipitation supercell storm, or HP to bow echo;
  - The classic supercell may appear to evolve into a high precipitation supercell as it decays, but the HP supercell distinguishes itself from the dissipating classic supercell by sustaining its rotation; and
  - HP supercells tend to be outflow dominated which undercuts the mesocyclone and limits the potential for long-lived tornadoes.

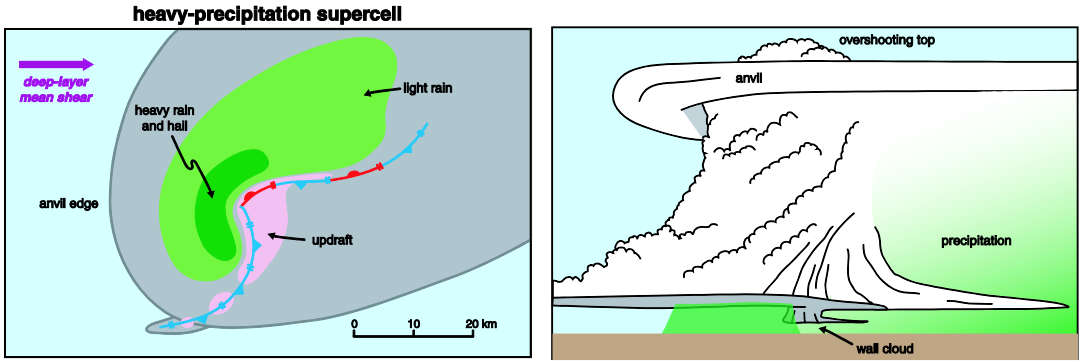

(Markowski & Richardson 2010)

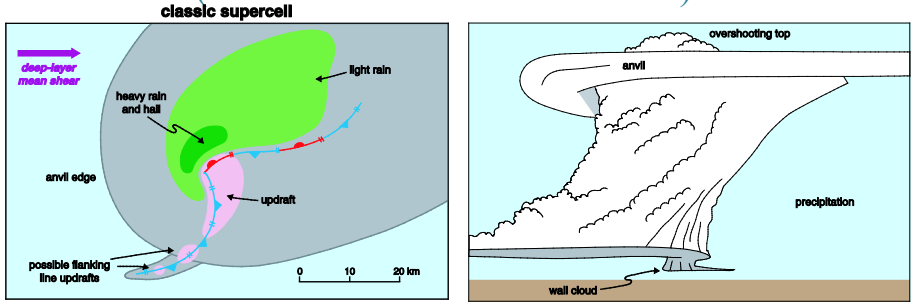

➢ The LP supercell storms normally form in the High Plains of the U.S. They possess the following common features:

- very few radar signatures compared to those observed for classic supercell storms,
- little (if any) precipitation falling under the cloud base; no evidence of strong downdraft at the surface,
- intense updrafts at the storm's rear flank and weak-to-moderate-intensity downdrafts,
- large hail falling outside the main cumuliform tower,
- few tornadoes produced because they have little to no RFD; and
- high LCL height may retard deep stretching of vorticity associated with mesocyclone. Major features associated with HP and LP storms have been reasonably well-simulated by nonlinear, nonhydrostatic cloud models.

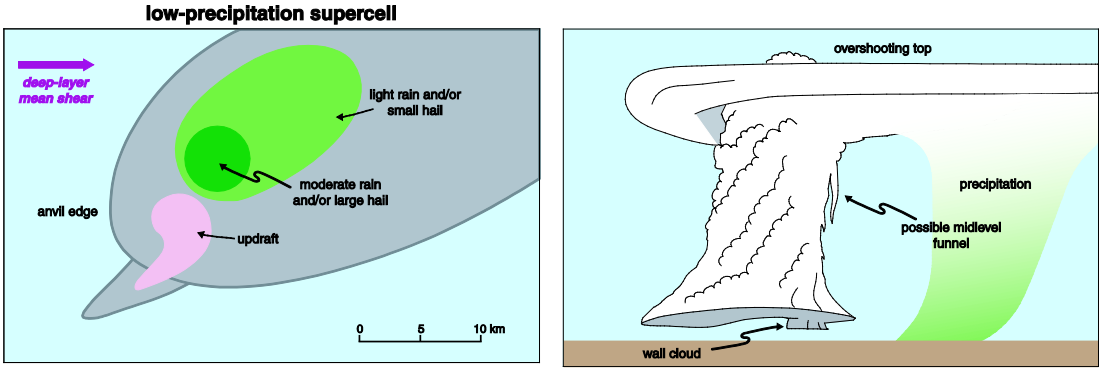

(Markowski & Richardson 2010)

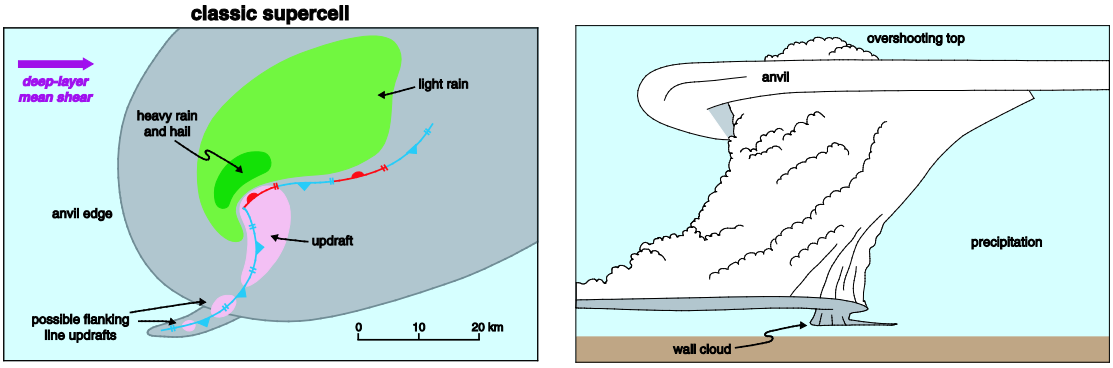

- A typical synoptic scale environment conducive to an outbreak of severe storms in the midlatitudes is depicted in the following:

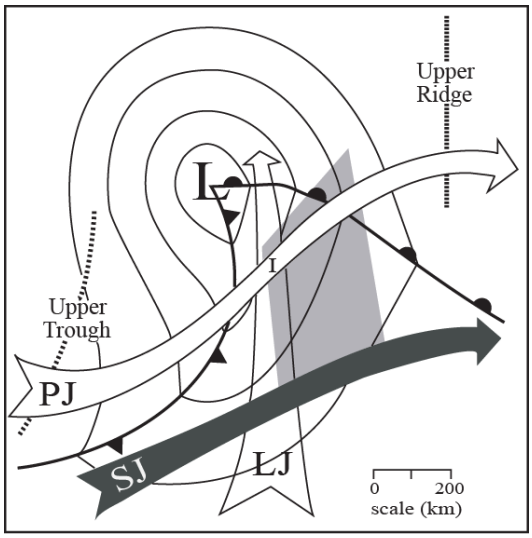

Fig. 8.10: A schematic of the synoptic environment conducive to severe convective storm outbreaks. Symbols are denoted as follows: LJ: low-level jet; PJ: polar jet; SJ: subtropical jet; I: intersection of PJ and LJ; and light-shaded area: area of severe convection. Surface features are denoted by conventional symbols. (After Barnes and Newton 1986)

Severe convective storms are considered most likely to occur in the warm sector of a surface cyclone (represented as the light-shaded area in the figure).

The region along and just north of the warm front is favorable for tornadogenesis.

Severe storms tend to form near the intersection of the polar jet and low-level jet (denoted as "I" in the figure). There is an upper-level synoptic wave oriented from southwest to northeast with the inflection point located right over the surface cyclone.

Supercell forecasting has advanced to be more quantitative, which is far beyond the conceptual model as shown in Fig. 8.10. Since this is a rapidly evolving subject of current research, it is only appropriate to provide a very brief summary.

Some important findings related to supercell storms are (e.g., Doswell 2001):

(a) Multiple control parameters are needed for making more accurate forecasting of supercell storms.
(b) Some control parameters include the storm relative helicity (SRH), vertical shear (e.g., $\Delta U = U_m - U_s$, i.e. surface–mid-level shear), CAPE, bulk Richardson number (R_B), buoyant RFD, low LCL (enhancing the ingest of high θ_e air into low-level mesocyclone), super composite parameter (combination of mid-level CAPE, 0 – mid-level shear and near-surface SRH).
(c) RFD has to remain buoyant (Markowski et al. 2002).
(d) Supercell environments are characterized by:
    (i) $\Delta U = U_{\mathrm{m}} - U_s > 15 - 20$ ms^{-1},
    (ii) $10 < R_B < 50$,
    (iii) 1000 $\mathrm{m}^2\mathrm{s}^{-2}$ < CAPE < 3500 $\mathrm{m}^2\mathrm{s}^{-2}$.

11.4.2 Effects of unidirectional shear

- If convection is initialized by an isolated thermal instead of a line thermal, as used in Section 8.3, the flow responses are more complicated. To elucidate this, consider a three-dimensional conditionally unstable flow with unidirectional shear.

- The soundings from these experiments are shown in Fig. 8.18a, where the surface water vapor mixing ratio is q_{vo} = 14 g kg^{-1}. The sounding has a CAPE of 2200 J kg^{-1}, which represents an environment of moderate conditional instability. The vertical wind profiles are assumed to be

$$U(z) = \Delta U \tanh\ (z / z_o), \qquad (8.4.1)$$

where z_o = 3 km, a constant throughout all the simulations, and ΔU is an averaged wind shear from the surface to 6 km (Fig. 8.18b).

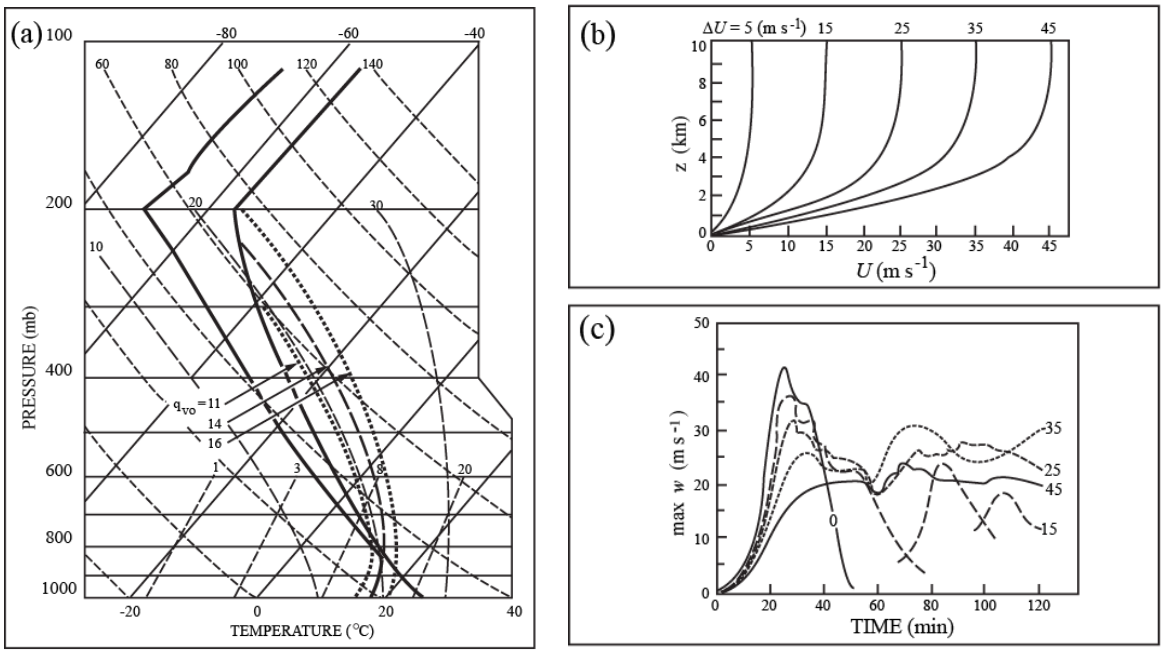

Fig. 8.18: Storm development in a three-dimensional, conditionally unstable, unidirectional shear flow. (a) Temperature and dew point profiles on a skew-T log-p diagram. The heavy dashed line denotes the moist adiabat following the air parcel ascent from the surface with a mixing ratio of q_{vo} = 14 g/kg. Heavy dotted lines denote similar parcel ascents for q_{vo} =11 g/kg and q_{vo} = 16 g/kg. Tilted solid lines are isotherms, short dashed lines are dry adiabatts, and long dashed lines are moist adiabats. (b) Wind profiles defined by (8.4.1). (c) Time series of maximum vertical velocities for wind shear experiments, in which the vertical wind profiles are depicted in (b) and q_{vo} = 14 g/kg. (After Weisman and Klemp 1982) [Lin 2007]

- Six wind profiles with ΔU varying from 0 to 45 ms^{-1} are used to investigate the sensitivity of the flow responses to differing shear strength.

- The convection is initiated by an isolated, spherical thermal with a radius of 10 km in the horizontal, a radius of 1.4 km in the vertical, and a +2 K temperature perturbation.

- The sensitivity to shear is illustrated by the time evolution of the maximum vertical velocities simulated for the above six cases (Fig. 8.18c).

➢ For zero vertical shear, the maximum *w* increases rapidly in the first 25 minutes and then decreases to almost 0 ms^{-1} in the next 25 minutes.

➢ For moderate shear, such as $\Delta U = 15$ ms^{-1}, distinct new convective cells are regenerated at the gust front of the density current, revealing a multicellular storm structure. The regeneration of convective storms can be explained by the RKW theory.

➢ The initial storm weakens rapidly as a result of precipitation loading associated with the rainfall, which cuts off the supply of potentially warm air needed for maintaining the updraft.

➢ Surface convergence is initially strongest on the right and left flanks of the storm; however, as the surface outflow spreads, deep lifting occurs along the gust front directly downshear (east) of the storm.

This leads to the formation of the second storm, which propagates downshear and reaches its maximum strength.

➢ Following the same redevelopment process, a third storm forms consecutively and reaches its maximum strength, but is weaker than the first and second storms.

- The redevelopment process is controlled by the competing forcings from the low-level shear and the density current, as discussed in the RKW theory in the Section 8.3.

- For a strong shear, such as $\Delta U \geq 25\ \mathrm{ms}^{-1}$, the storm redevelopment is replaced by a regime of *storm splitting*. The storm splitting dynamics will be discussed in subsection 8.4.4.

- In this regime, the initial updraft is split into right- (facing downshear) and left-moving storms.

  A pair of equal, self-maintaining storms are produced in a relatively continuous fashion on both the right and left (facing downshear) flanks of the original storm's outflow boundary.

  The updraft of the right (left) moving storm is flanked by a cyclonic (anticyclonic) vorticity. The right-moving storm (Fig. 8.19) behaves like a supercell storm.

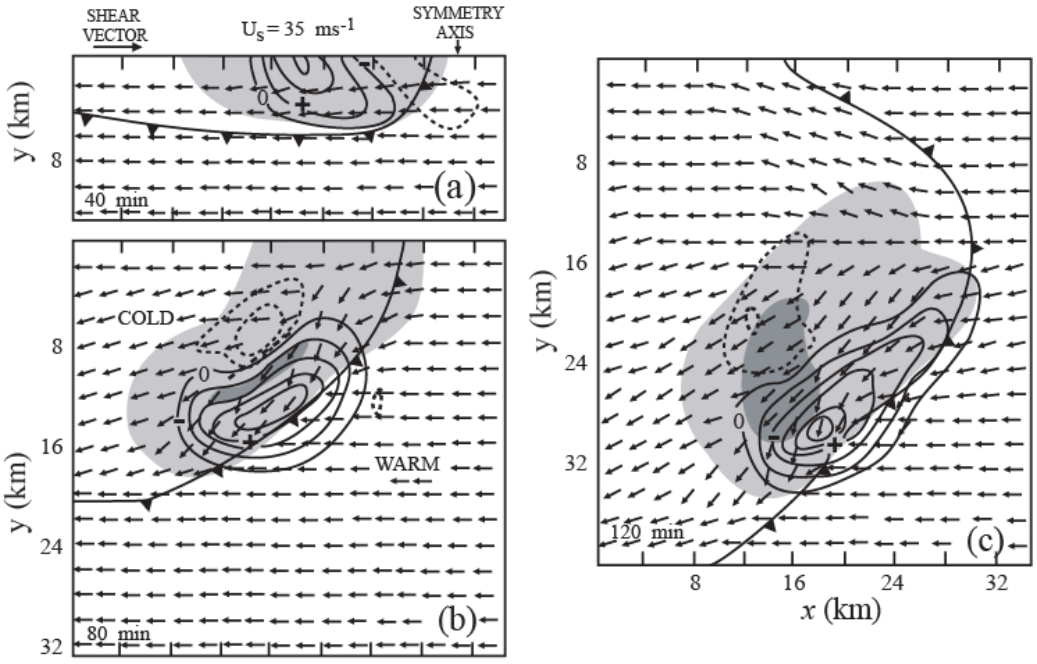

Fig. 8.19: Storm development in a three-dimensional, conditionally unstable, strong shear flow where U_o = 35 ms^{-1}and q_{vo} = 14 g/kg (see Fig. 8.16a) at (a) 40 min, (b) 80 min, and (c) 120 min. Displayed in the figures are: the horizontal wind vectors at lowlevel (z = 178 m), surface rain indicated by light shading, the dark shading indicates rain areas > 4 g kg^{-1}, mid-level (z = 4.6 km) w contoured every 5 ms^{-1} (2 ms^{-1}) for upward (downward) motion, and the surface gust front (represented by -0.5^{o}C temperature perturbation and denoted by the solid barbed line). Positive signs denote the location of local low-level w_{max} . Only the southern half of the domain on a moving frame of reference is shown. Note that the storm splits into right (southward) and left moving storms. (After Weisman and Klemp 1982) [Lin 2007]

- The maximum vertical velocity of the initial updraft decreases as shear increases, which may be attributed to the advection effect by the basic wind (Fig. 8.18c).

- The maximum w of a split storm oscillates at about the same value at later times compared to initial times, in response to the redevelopment process of the storm. The storm splitting process can be clearly seen for $U_S = 35$ ms^{-1} (Fig. 8.19).

- Unlike the weak shear case, no westerly surface outflow has developed behind the gust front (Figs. 8.19b-c).

  This lack of outflow weakens the ability for the secondary storm to redevelop. On the other hand, the increased shear has enhanced the process of storm splitting, as evidenced by the stronger maximum vertical velocity (Fig. 8.18).

- With a unidirectional shear, the left-moving storm is simply a mirror image of the right-moving storm.

  In order for a steady split storm to develop, the storm-relative inflow shear must be strong enough to keep the density current from propagating away from the updraft.

  The right-moving storm becomes dominant when the vertical shear is directional and clockwise and is also referred to as the *severe right* (*SR*) *storm* or *right mover*.

11.4.3 Storm splitting

- As discussed earlier, storm redevelopment falls into the regime of *storm splitting*, as the unidirectional vertical shear increases (Figs. 8.14c and 8.19).

  Near the end of the initial updraft, a pair of equal, self-maintaining storms is produced in a relatively continuous fashion on both the right and left (facing downshear) flanks of the original storm's updraft.

- Figure 8.20 contains a three-dimensional schematic depicting storm splitting and rotation development.

  - During the early stage of storm development, tilting of horizontal vorticity associated with the environmental shear (westerly shear in this case) causes a pair of vortices to form.

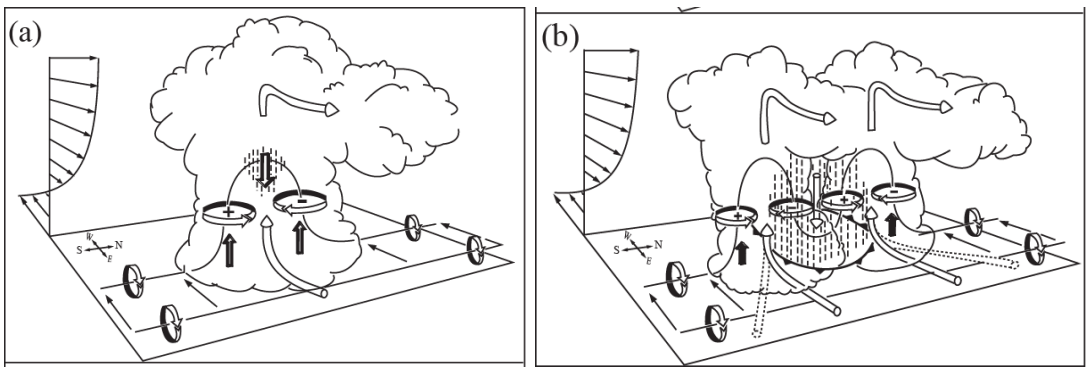

Fig. 8.20: A schematic depicting rotation development and the storm splitting. (a) Rotation development: In the early stage, a pair of vortices forms through tilting of horizontal vorticity associated with the (westerly) environmental shear. (b) Storm splitting: In the later stage, the updraft is split into two convective cells by the upward pressure gradient forces. See text for details. Cylindrical arrows denote the direction of the storm-relative airflow, and heavy solid lines represent vortex lines with the sense of rotation denoted by circular arrows. Shaded arrows represent the forcing promoting new updraft and downdraft acceleration. Vertical dashed lines denote regions of precipitation. Frontal symbols at the surface mark the boundary of cold air outflow. (After Klemp 1987; Reprinted, with permission, from the Annual Review of Fluid Mechanics, Vol. 19 @1987 by Annual Reviews) [Lin 2007]

- During the later stage of storm development, precipitation accumulates within the updraft, thus resulting in increasingly negative buoyancy that produces a downdraft within the cloud.

- If the environmental shear is strong, then the upward pressure gradient forces reinforce new updraft growth on the southern and northern flanks of the original updraft center.

  The upward pressure gradient forces then gradually split the updraft into two convective cells that move rightward (southward) and leftward (northward) with respect to the shear vector. At this stage, vortex lines are tilted downward, producing two vortex pairs.

➢ The upward pressure gradient force may be understood by analyzing the vertical momentum equation.

By partitioning the pressure into a buoyancy component (p'_{b}) and a dynamic component (p'_{d}), the vertical momentum equation (7.3.8)

$$\frac{Dw}{Dt} = -\frac{1}{\bar{\rho}}\frac{\partial p'_d}{\partial z} + \left(b - \frac{1}{\bar{\rho}}\frac{\partial p'_b}{\partial z} \right), \tag{7.3.8}$$

where b is the buoyancy and p'_d and p'_b are derived from the Bossinesq form of the momentum equation (Rotunno and Klemp 1985; Emanuel 1994),

$$-\frac{1}{\bar{\rho}}\nabla^2 p'_d = |D|^2 - |\boldsymbol{\omega}|^2, \tag{7.3.9}$$

$$-\frac{1}{\bar{\rho}}\nabla^2 p'_b = -\frac{\partial b}{\partial z}. \tag{7.3.10}$$

and where $|D|$ is the magnitude of the total deformation (see (8.4.9) for the mathematical definition) and $\boldsymbol{\omega}$ is the three-dimensional vorticity vector.

may be rewritten as

$$\underbrace{\frac{\partial w}{\partial t}}_{(1)} = \underbrace{-\boldsymbol{v}\cdot\nabla w}_{(2)} \underbrace{-\frac{1}{\overline{\rho}}\frac{\partial p'_{\mathrm{d}}}{\partial z}}_{(3)} \underbrace{-\left(\frac{1}{\overline{\rho}}\frac{\partial p'_{\mathrm{b}}}{\partial z} - b\right)}_{(4)}, \qquad (8.4.2)$$

1. vertical acceleration
2. advection
3. dynamic forcing
4. buoyancy forcing

($\boldsymbol{v}$ is the three-dimensional velocity vector, $\overline{\rho}$ is the basic state density, and b is the buoyancy.)

As often adopted in storm dynamics, the full *buoyancy* is defined as

$$b \equiv g\left[\frac{\theta'}{\overline{\theta}} + 0.61 q_v' - q_T\right], \qquad (8.4.3)$$

where

θ': perturbation potential temperature
q_v': perturbation water vapor mixing ratio
q_T: mixing ratio of total hydrometeors in the air

[The last term inside the bracket includes the *precipitation loading* effects.]

Note that the buoyancy forcing should include both terms inside the bracket on the right hand side of (8.4.2) because $b > 0$ includes a compensating downward buoyant pressure gradient force.

Taking the divergence of the nonrotating (f=0) equation of motion

$$\frac{\partial \boldsymbol{v}}{\partial t} = -\boldsymbol{v}\cdot\nabla\boldsymbol{v} - \frac{1}{\overline{\rho}}\nabla p' + b\boldsymbol{k}, \qquad (8.4.4)$$

and using the anelastic continuity equation,

$$\nabla \cdot (\bar{\rho}\boldsymbol{v}) = 0\,, \tag{8.4.5}$$

leads to

$$\nabla^2 p' = -\nabla \cdot (\bar{\rho}\boldsymbol{v} \cdot \nabla \boldsymbol{v}) + \frac{\partial(\bar{\rho} b)}{\partial z}\,. \tag{8.4.6}$$

With the partition of $p' = p'_{\mathrm{d}} + p'_{\mathrm{b}}$, we have

$$\nabla^2 p'_{\mathrm{d}} = -\nabla \cdot (\bar{\rho}\boldsymbol{v} \cdot \nabla \boldsymbol{v})\,, \tag{8.4.7}$$

$$\nabla^2 p'_{\mathrm{b}} = \frac{\partial(\bar{\rho} b)}{\partial z}\,, \tag{8.4.8}$$

subjected to the Neumann boundary conditions $\partial p'_{\mathrm{d}} / \partial z = 0$ and $\partial p'_{\mathrm{b}} / \partial z = b$ at $z = 0, z_T$, where z_T is the top of the domain considered.

Applying the anelastic continuity equation (8.4.5) to (8.4.7) gives

$$\nabla^2 p'_{\mathrm{d}} = \bar{\rho}\left(|\boldsymbol{\omega}|^2 - |D|^2\right),$$

$$|\boldsymbol{\omega}|^2 = (w_y - v_z)^2 + (u_z - w_x)^2 + (v_x - u_y)^2\,,$$

$$|D|^2 = (u_x^2 + u_y^2 + u_z^2) + (v_x^2 + v_y^2 + v_z^2) + \{(w_x^2 + w_y^2 + w_z^2) - (d \ln \bar{\rho}/dz)\boldsymbol{v} \cdot \nabla w - (d^2 \ln \bar{\rho}/dz^2) w^2\}\,. \tag{8.4.9}$$

In (8.4.9),

$\boldsymbol{\omega} \equiv \nabla \times \boldsymbol{v}$: 3D vorticity vector

$|D|$: magnitude of the *total deformation*

{=sum of *shear deformation* (e.g., u_y and u_z) and *stretching deformation* (e.g., u_x)}

In a thunderstorm with strong vertical vorticity, such as a supercell storm, the right-hand side of (8.4.9) is dominated by $v_x u_y$.

For a horizontal wind field with pure rotation, in which $v_x = -u_y$, then $v_x u_y \approx -1/4\zeta^2$, where ζ is the vertical vorticity.

Assuming sinusoidal variations in a flow's interior, the Laplacian of a variable is roughly proportional to the negative of the variable itself, i.e. $\nabla^2 p'_{\mathrm{d}} \propto -p'_{\mathrm{d}}$, if the vertical variations of density and virtual potential temperature are neglected on the left side of (8.4.9). This leads to

$$p'_{\mathrm{d}} \propto -\zeta^2 . \qquad (8.4.10)$$

Thus, a dynamically perturbed low pressure is associated with a vortex, regardless of whether the vortex is cyclonic or anticyclonic.

[Experiment: Stir the water in a bucket with a stick clockwise and counterclockwise to see what happens.]

In other words, to a first-order approximation, the flow tends to adjust to *cyclostrophic flow* balance, where, in absence of the Earth's rotation, the pressure gradient force is balanced by the centrifugal force.

Note that an upward motion is associated with convergence near a flat lower surface through vertical stretching as required by the mass continuity in an anelastic or incompressible fluid.

This upward motion does not require a vertical acceleration (*Dw/Dt*) from the imbalance between the vertical pressure gradient force and the buoyancy force in the vertical momentum equation.

On the other hand, the relationship (i.e., mass continuity) between the vertical motion and near surface convergence is diagnostic, thus the causality is unclear and may deserve a further study.

During the early stage of supercell storm development, a pair of midlevel vortices forms through tilting of horizontal vorticity associated with the strong environmental shear (Fig. 8.20a).

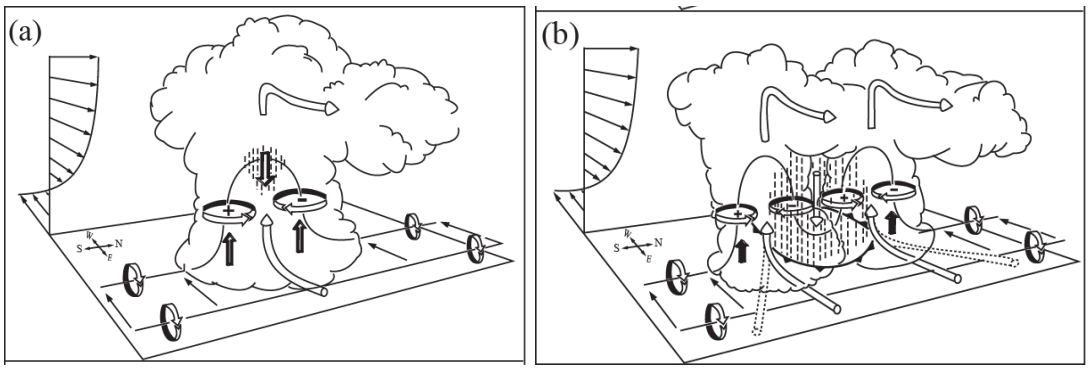

Fig. 8.20: A schematic depicting rotation development and the storm splitting.
(a) Rotation development: In the early stage, a pair of vortices forms through tilting of horizontal vorticity associated with the (westerly) environmental shear.
(b) Storm splitting: In the later stage, the updraft is split into two convective cells by the upward pressure gradient forces.
See text for details. Cylindrical arrows denote the direction of the storm-relative airflow, and heavy solid lines represent vortex lines with the sense of rotation denoted by circular arrows. Shaded arrows represent the forcing promoting new updraft and downdraft acceleration. Vertical dashed lines denote regions of precipitation. Frontal symbols at the surface mark the boundary of cold air outflow. (After Klemp 1987; Reprinted, with permission, from the Annual Review of Fluid Mechanics, Vol. 19 @1987 by Annual Reviews) [Lin 2007]

(8.4.10) =>

(1) Tilting of horizontal vorticity generates strong rotation with midlevel vortices (mesocyclone)

(2) Lowers pressure at the vortex center via (8.4.10): $p'_{\mathrm{d}} \propto -\zeta^2$

(3) Induces acceleration in the updraft on each flank of the storm, according to (8.4.2):

$$\frac{\partial w}{\partial t} = -\boldsymbol{v}\cdot\nabla w - \frac{1}{\overline{\rho}}\frac{\partial p'_{\mathrm{d}}}{\partial z} - \left(\frac{1}{\overline{\rho}}\frac{\partial p'_{\mathrm{b}}}{\partial z} - b\right)$$

(4) The strengthening updrafts then split the initial updraft into two, creating the storm split (Fig. 8.20b).
(5) When the storm matures, the precipitation-induced strengthening downdraft tilts the vortex line downward and helps produce an additional pair of vortices.
(6) This facilitates propagation of the split storm away from the original storm center.

Based on observations and the schematic in Fig. 8.20, one may suspect that precipitation-induced downdraft causes storm splitting and propagation. However, numerical simulations have demonstrated that even in the absence of precipitation (which prevents formation of the central downdraft), updraft splitting still occurs.

11.4.4 Storm rotation and propagation

To illustrate rotational development in a supercell storm, consider the momentum equation, (8.4.4), and the anelastic continuity equation, (8.4.5). If we take the curl of (8.4.4)

$$\frac{\partial \boldsymbol{v}}{\partial t} = -\boldsymbol{v}\cdot\nabla\boldsymbol{v} - \frac{1}{\bar{\rho}}\nabla p' + b\boldsymbol{k}\,, \qquad (8.4.4)$$

and note that the curl of the gradient vanishes, we then find the three-dimensional vorticity equation

$$\frac{\partial \boldsymbol{\omega}}{\partial t} = \nabla \times (\boldsymbol{v} \times \boldsymbol{\omega}) + \nabla \times (b\boldsymbol{k})\,. \qquad (8.4.12)$$

The local rate of change of the vertical vorticity, $\zeta = \boldsymbol{k}\cdot\boldsymbol{\omega}$, can then be obtained by taking $\boldsymbol{k}\cdot(8.4.12)$

$$\frac{\partial \zeta}{\partial t} = -\boldsymbol{v}\cdot\nabla\zeta + \left(\frac{\partial u}{\partial z}\frac{\partial w}{\partial y} - \frac{\partial v}{\partial z}\frac{\partial w}{\partial x}\right) + \zeta\frac{\partial w}{\partial z}\,. \qquad (8.4.13)$$

vorticity advection

tilting of the horizontal vorticity

vertical vorticity stretching

- Both the advection and stretching terms require pre-existence of the vertical vorticity.
- The only initial source of vertical vorticity in a non-rotating system is therefore the tilting of the horizontal vorticity.
- The rotation of the Earth does not play an important role in storm dynamics and is therefore omitted from the basic equations.

- Horizontal vorticity is contained in the environmental shear and is characterized by the *environmental wind-shear vector*, $\boldsymbol{S} = d(\boldsymbol{V} - \boldsymbol{c})/dz$, where $\boldsymbol{V} - \boldsymbol{c}$ is the *storm-relative environmental wind velocity*.

- The shear vector consists of two components, namely the *speed shear* and the *directional shear*.

  Speed shear is a change in wind speed with height while directional shear is a change in wind direction with height.

  Mathematically, the storm-relative wind vector can be expressed as $\boldsymbol{V} - \boldsymbol{c} = |\boldsymbol{V} - \boldsymbol{c}|\,\boldsymbol{p}$, where $\boldsymbol{p}$ is the unit vector in the direction of $\boldsymbol{V} - \boldsymbol{c}$, and the shear vector becomes

$$\boldsymbol{S} = \frac{d(\boldsymbol{V} - \boldsymbol{c})}{dz} = \frac{d|\boldsymbol{V} - \boldsymbol{c}|}{dz}\boldsymbol{p} + |\boldsymbol{V} - \boldsymbol{c}|\frac{d\boldsymbol{p}}{dz}. \qquad (8.4.14)$$

  The speed shear and directional shear are represented by the first and second terms on the right hand side of (8.4.14).

➢ The directions of the shear vector in a composite hodograph are illustrated in Fig. 8.21.

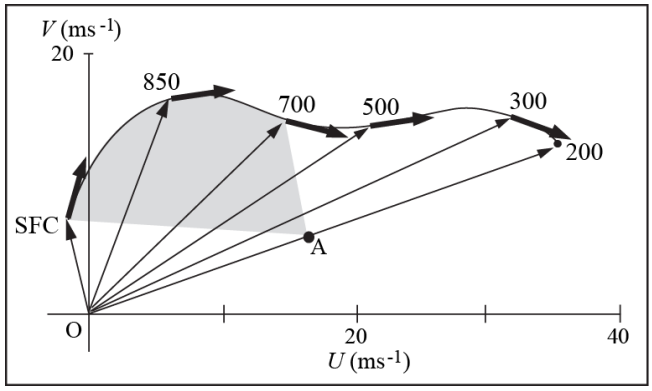

Fig. 8.21: A composite sounding of wind hodograph from 62 tornado outbreak cases. The winds are computed at each level relative to the estimated storm motion. Heavy arrows denote the direction of the shear vector at each level (in hPa). The estimated mean storm motion is denoted

by the vector OA. The shaded area is proportional to the 0 – 3 km storm-relative environmental helicity (Davies-Jones 1984, adapted after Maddox 1976)

- Figure 8.22a shows an example of a shear vector that contains only the speed shear. In this figure, *S* is oriented parallel to the line LMH. Directional shear, such as that shown in Fig. 8.22b, plays an essential role in affecting the storm rotation and propagation.

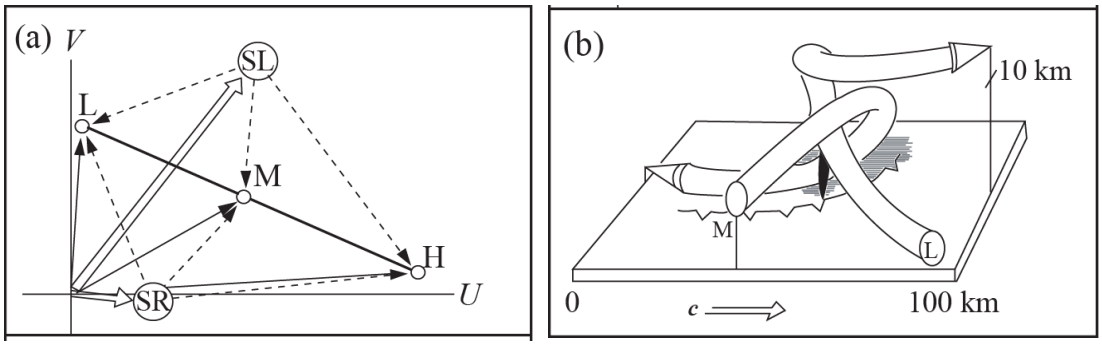

- Storm dynamics are highly nonlinear and complex, which prohibits a closed form of analytical theory even in its linear form.

  However, a few basic dynamics of storms can still be understood by studying the linear dynamics.

  For example, vertical tilting of the horizontal vorticity can be understood by considering the linearized form of the tilting term in (8.4.13), $(\partial U/\partial z)(\partial w/\partial y)-(\partial V/\partial z)(\partial w/\partial x)$, where *U* and *V* are the basic wind speeds.

  Now consider the situation shown in Fig. 8.20a where positive horizontal vorticity is associated with the environmental wind shear ($\partial U/\partial z>0$; $V=0$ and $\partial V/\partial z=0$).

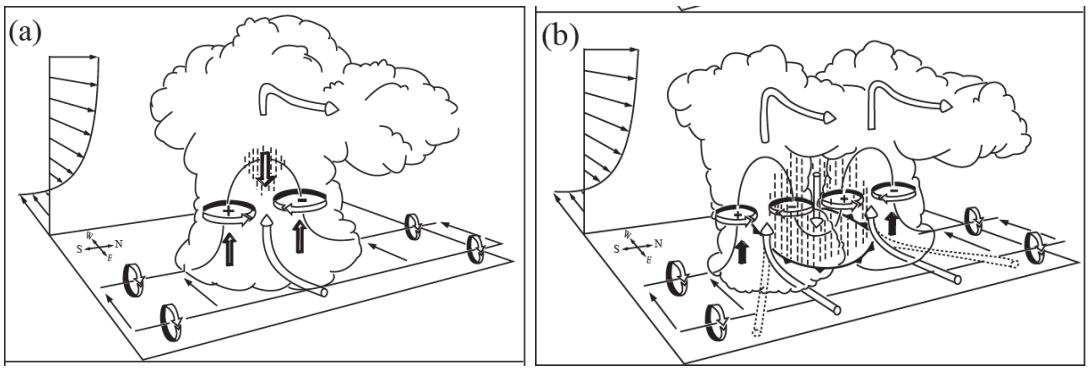

Fig. 8.20: A schematic depicting rotation development and the storm splitting.
(a) Rotation development: In the early stage, a pair of vortices forms through tilting of horizontal vorticity associated with the (westerly) environmental shear.
(b) Storm splitting: In the later stage, the updraft is split into two convective cells by the upward pressure gradient forces.

This horizontal vorticity is then tilted into the vertical when the vortex tube encounters the updraft ($\partial w/\partial y > 0$), thus generating the positive vertical vorticity shown at the southern flank of the storm.

Similarly, a negative vertical vorticity is generated on the northern flank of the storm in the area where $\partial w/\partial y < 0$.

- The rotation and propagation of supercell storms may be understood from the streamwise vorticity and helicity point of view.

When an isentropic surface bulges up by an updraft, it may be represented by the "peak" of a θ_e surface, as sketched in Fig. 8.23.

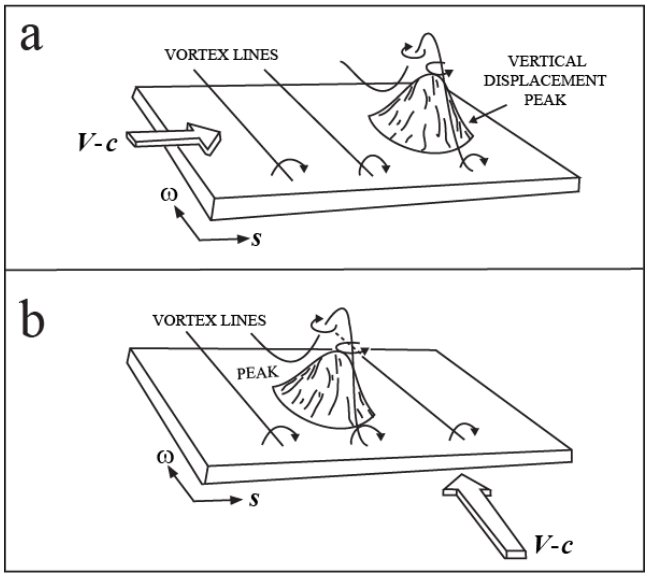

Fig. 8.23: Effects of a localized updraft, represented by the vertical displacement "peak" (i.e. "hump" in isentropic surface), on vortex lines when environmental vorticity $\boldsymbol{\omega}$ and storm-relative mean flow ($\boldsymbol{V} - \boldsymbol{c}$) are (a) perpendicular and (b) parallel, which will produce pure crosswise environmental vorticity and pure streamwise environmental vorticity, respectively. (From Davies-Jones 1984)

- For the situation in Fig. 8.23a, the storm-relative mean flow ($\boldsymbol{V} - \boldsymbol{c}$) is perpendicular to the environmental vorticity vector ($\boldsymbol{\omega}$), which is called *crosswise vorticity*.

  Note that *c* is the storm translation velocity or motion vector. The vortex lines are forced to go up over the peak, giving rise to a cyclonic vorticity on the right-hand side (facing downshear) of the peak and an anticyclonic vorticity on the left hand side of the peak.

  The updraft (downdraft) is located upstream (downstream) of the peak in the storm-relative moving frame. In this case, there is no correlation between vertical velocity and vertical vorticity.

- On the other hand, in the situation of Fig. 8.23b, the storm-relative mean flow ($\boldsymbol{V} - \boldsymbol{c}$) is parallel to the environmental vorticity vector ($\boldsymbol{\omega}$), which is called *streamwise vorticity*.

  The upslope (downslope) side of the peak is also the cyclonic (anticyclonic) side. The vertical velocity and vertical vorticity are

correlated. Thus, the supercell storm motion may lead to the generation of helical updraft rotation via vertical tilting of the *environmental streamwise vorticity*, which is defined as

$$\zeta_s = \frac{(\boldsymbol{V} - \boldsymbol{c}) \cdot \boldsymbol{\omega}}{|\boldsymbol{V} - \boldsymbol{c}|} \,. \qquad (8.4.15)$$

In fact, the tendency of an environment to produce a rotating storm can be measured by a quantity called the *storm-relative helicity* (Lilly 1986) which is defined as the integration of the streamwise vorticity times the storm-relative flow speed through *h*, the depth of the primary inflow layer of the storm:

$$H(\boldsymbol{c}) = \int_0^h (\boldsymbol{V} - \boldsymbol{c}) \cdot \boldsymbol{\omega} \, dz \,. \qquad (8.4.16)$$

- Helicity is conserved for an inviscid and homogeneous fluid. A rotating storm requires a high correlation between the storm-relative velocity and the streamwise vorticity, which therefore requires a high helicity for the environmental wind.

Since $\boldsymbol{\omega} \approx \boldsymbol{k} \times d\boldsymbol{V}/dz$, the *storm-relative environmental helicity* (*SREH*), (8.4.16), may also be defined as (Davies-Jones 1984):

$$H(\boldsymbol{c}) = -\int_0^h \boldsymbol{k} \cdot (\boldsymbol{V} - \boldsymbol{c}) \times \frac{d\boldsymbol{V}}{dz} dz \,. \qquad (8.4.17)$$

The 0-3 km SREH can be calculated as twice the area swept out by the storm-relative wind vector between the surface and 3 km in a hodograph (shaded area in Fig. 8.21). Approximate ranges of SR helicity favorable for weak, strong and violent right movers are found to be 150 - 299 m^2s^{-2}, 300-449 m^2s^{-2} and greater than 450 m^2s^{-2}, respectively.

In addition, the concurrent presence of high SR helicity values and the existence of long-lived updrafts imply strong right movers, which may favor tornadogenesis. Thus, SREH may serve as an index for supercell forecasting and potential tornado warming.

11.2.5 Effects of directional shear

As briefly mentioned in Section 8.4.1, cyclonically rotating, right-moving storms, often referred to as the severe right (SR) storms or right movers, are dominant when the vertical shear is directional and clockwise. In fact, anticyclonically rotating, left-moving storms are rarely observed. Observations indicate that the majority of supercell storms in the United States rotate cyclonically. This bias is not directly due to the Coriolis force, however. Instead, it results from the fact that the low-level shear vector turns anticyclonically with height throughout most of the midlatitudes. This orientation of the wind profiles, in turn, is influenced by the sign of the Coriolis parameter. This directional shear is clearly shown in the composite sounding of tornadic thunderstorms in the central United States (Fig. 8.21).

Figure 8.24 shows, for two completely different wind profiles, how a numerically simulated storm evolves in the absence of the earth's rotation and surface drag. One profile has a unidirectional shear, i.e. a straight-line hodograph, and the other exhibits a directional shear, i.e., a curved-line hodograph, which is representative of a clockwise turning of the wind-shear vector with height. In the case of unidirectional shear, the initial storm splits into two storms after 40 min. The storms move apart as they propagate towards the northeast. As can be seen from the figure, they evolve into two almost identical, mirror-image right- and left-moving storms. When there is clockwise turning of the wind-shear vector with height, however, the cyclonically rotating, right-moving storm evolves into an intense storm while the anticyclonically rotating, left-moving storm cannot develop any further and is short-lived. The key factor in storm longevity is the turning of the wind-shear vector, as opposed to the wind vector. The wind vector turns in a clockwise direction in both cases, and does not directly influence the length of the storm's lifetime.

The means by which directional shear enhances the right-moving storm can be explained by examining the linear dynamic pressure equation of (8.4.9),

$$\nabla^2 p'_{\mathrm{d}} = -2\bar{\rho}\, \boldsymbol{S} \cdot \nabla_{\mathrm{H}} w \qquad (8.4.18)$$

where $\boldsymbol{S}$ is the shear vector as defined in (8.4.14). Since the Laplacian of a variable is roughly proportional to the negative of the variable itself in the flow interior, (8.4.18) implies

$$p'_{\mathrm{d}} \propto \boldsymbol{S} \cdot \nabla_{\mathrm{H}} w\,. \qquad (8.4.19)$$

Therefore, within the context of linear theory, the interaction between the updraft and the shear flow produces high (low) pressure on the upshear (downshear) side of the maximum region of the updraft, as seen in the directional shear figure (Fig. 8.25b). In other words, a high-to-low pressure gradient develops across the updraft in the direction of local shear vector. Since the vertical velocity and the gradient of w bounding it are strongest at midtroposphere, this pressure perturbation is also strongest at that level. The cumulative strength of all three produces an upward pressure-gradient acceleration in the lower troposphere on the downshear side of the storm. In the unidirectional shear case (Fig. 8.25a), an eastward (downshear) high-to-low pressure gradient force is produced because the shear vector points eastward at all levels. As the updraft intensifies, these pressure perturbations reinforce inflow on the downshear (east) side. However, they do not contribute to any preferential growth on either side of the storm.

12.5 Tornado dynamics

12.5.1 Supercell tornadogenesis

Based on measured local circulations and wind speeds, the tornado is the most intense type of circulation observed in the atmosphere. A tornado vortex has a typical diameter of a few hundred meters and a maximum tangential wind speed of up to 140 ms^{-1}. Observations show that most intense tornadoes are produced by supercell storms, although not all supercell storms produce tornadoes. Out of the 5322 individual mesocyclones detected by Doppler radars, only 26% were associated with tornadoes (e.g., Trapp et al. 2005). A tornado occurring in a rotating supercell storm is often referred to as a *supercell tornado*. Supercell tornadoes are preceded by a deep persistent mesocyclone of a mean diameter 3 – 9 km and a vertical vorticity that is typically greater than 0.01 s^{-1}. Tornadoes that occurr in the absence of mesocyclones are referred to as *nonsupercell tornadoes*.

When a supercell storm transitions into its tornadic phase, the storm's circulation and quasi-steady structure experience a significant alteration. Based on observations, the following processes have been found to be associated with the evolution of the mesocyclone and updraft: (1) a rapid increase in low-level rotation, (2) a decrease in updraft intensity, (3) a small-scale downdraft forming behind the updraft, and (4) a low-level flow in which outflow and inflow air spiral around the circulation center. A low-level mesocyclone acquires its rotation by vertically tilting the baroclinically-generated horizontal vorticity via the updraft and a combination of both the updraft and downdraft. The baroclinicity and updraft come from the forward flank outflow boundary.

During tornadogenesis, the low-level flow behaves in a similar manner to that shown in Fig. 8.26. Tornadogenesis within a supercell storm is often preceded by the development of a *rear flank downdraft* (RFD) on the upshear side of the updraft. On the forward (downshear) flank of the updraft, another area of downdraft, i.e. forward flank downdraft (FFD), is generated by evaporative cooling. Along the edge of the FFD, horizontal vorticity is baroclinically produced along the boundary between warm and cold

air (on the south and north side, respectively). The vorticity is tilted upward into the updraft (denoted by encircled "T" in Fig. 8.26). The vertical vorticity associated with the low-level mesocyclone amplifies as the air column is stretched by the updraft. The boundary between RFD and the warm inflow from the southeast, and the FFD and the warm inflow from the east, behaves like a *storm-scale frontal system*. As the RFD intensifies the downdraft outflow progresses cyclonically around the center of rotation which circles around the updraft. The updraft and rotation associated with the mesocyclone may develop to tornado intensity and form a tornado. Recent in situ surface observations indicate that:

(a) tornadogenesis is more likely and tornado intensity and longevity increase as the surface buoyancy, potential buoyancy (measured by CAPE), and equivalent potential temperature in the rear RFD increase, and as the convective inhibition associated with RFD parcels at the surface decreases;

(b) evaporative cooling and entrainment of midlevel potentially cold air may play smaller roles in the development of RFDs associated with tornadic supercells compared to nontornadic supercells;

(c) environments characterized by very moist boundary layer air and a low cloud base may be more conducive to RFDs associated with relatively high buoyancy than environments characterized by very dry boundary layer air and a high cloud base; and

(d) baroclinity at the surface within the hook echo is not a necessary condition for tornadogenesis (Markowski et al. 2002).

The *tornado vortex* is visible as a *funnel cloud* extending down from the rotating *wall cloud* base. Lowering of pressure in the intense vortex causes water vapor to condense, which then causes the formation of a funnel cloud. The wall cloud is the lifting condensation level of air from the forward flank, which is lower than that of environmental inflow. An intense supercell updraft prevents precipitation from forming until the air parcels have ascended to higher levels. A hook-shaped *echo* or

vault appears in radar images (Figs. 8.16 and 8.17). Sometimes, if the updraft is intense, the WER becomes bounded and is referred to as BWER. A hook-shaped echo or hook echo (Fig. 8.17) may form as the mesocyclone advects precipitation away from the precipitation core and around the updraft. The formation of a hook echo serves as a precursor for predicting the location of a tornado. Since the winds of a mesocyclone are cyclonic, the reflectivity signature of a hook echo will have a cyclonically shaped hook. Inside the hook, the only area free from reflectivity is the updraft and inflow notch region of the supercell. Many of the violent tornadoes associated with classic supercells will show a distinct hook echo. Before tornado touchdown at the surface, Doppler radar may detect a local horizontal shear region, which is referred to as the *tornadic vortex signature* (TVS). Not all tornadoes have detectable TVS, especially for those that build upward (Trapp et al. 1999). In this type of tornado, the mesocyclone occludes as the RFD cuts off the supply of warm moist air, causing the original updraft to weaken. Although the supercell storm can persist in a quasi-steady configuration for up to several hours, the tornadogenesis process usually occurs in less than 10 minutes.

Many observed features of tornadic storms have been reproduced by cloud model simulations. Figure 8.27 shows the flow fields near the surface as simulated by a cloud model. The model uses a horizontal resolution of 120 m and a stretched grid in the vertical with a resolution of 120 m near the surface. At this time of simulation, the tornado is at its most intense stage, which is located at (x, y) = (28.8, 36.0 km) (Fig. 8.27a). There are two maximum areas of vertical velocity, one associated with the tornado and the other associated with the gust front. The rear-flank downdraft, initially located to the northwest of the mesocyclone, merges with the occlusion downdraft. An *occlusion downdraft* is a small scale downdraft that occurs during the collapse phase of a supercell as the gust front occludes with the stationary boundary, where warm inflow air is meeting outflow from the downdraft at the front flank of the supercell (Klemp et al. 1981). It is hypothesized that the RFD brings rotation to the surface initially, and then the gust front occludes. The occlusion process causes a tightening of low-level cyclonic

vorticity, intensifying the preexisting downdraft (Markowski et al. 2002). A column of vertical vorticity greater than 0.125 s^{-1} extends from the surface to a height of about 4 km (Fig. 8.27b). A surface meso-low of -17.3 hPa is produced (Fig. 8.27c) and collocated with the peak vorticity. The maximum storm-relative wind at this level (100 m) exceeds 45 ms^{-1}, while the maximum ground-relative wind speed exceeds 60 ms^{-1} (Fig. 8.27d). Prior to tornadogenesis, updrafts in the northern half of the mesocyclone intensify rapidly, causing the mesocyclone circulation to shrink in diameter. The tornado's decay begins when the surrounding updrafts weaken and the occlusion downdraft moves in on the tornado.

11.5.2 Nonsupercell tornadogenesis

Although the most intense long-lasting tornadoes are found to form within a supercell thunderstorm, *tornadoes may also form within a nonsupercell thunderstorm*. In other words, *a mid-level mesocyclone is not a necessary condition for tornadogenesis*. Nonsupercell tornadoes often occur along a stationary or slowly moving front, or in a horizontal windshift line. They are also referred to as *gust-front tornadoes*, or *type II tornadoes*; *type I tornadoes* form within a supercell thunderstorm. Some of their parent vortices are associated with *misocyclones*, which have diameters of less than 4 km.

This type of nonsupercell tornado can occur over water, and are referred to as *waterspouts*. They may last for as long as 20 – 30 min. Some waterspouts are spun up by supercells over water, while others may occur in cloud lines along sea breeze fronts. When these types of nonsupercell tornadoes occur over land, they are referred to as *landspouts*. Landspouts acquire their vorticity from the boundary layer and their parent clouds do not contain a preexisting midlevel mesocyclone. Landspouts have been observed in eastern Colorado along the Denver convergence-vorticity zone, and also over mountainous areas. In addition, it has been observed that the vorticity of nonsupercell tornadoes may be augmented by the vertical tilting of baroclinically generated vorticity, which is an important factor in the vorticity

generation of supercell tornadoes. Two or more waterspouts or landspouts may exist simultaneously along a line of clouds.

Figure 8.28 shows a conceptual model of a nonsupercell tornado lifecycle. In the initial stage, several small vortices, labeled A, B, and C in the figure, are generated by shear instability that results from horizontal shear across the boundary. It has been proposed that shear instability is responsible for generating initial vortices for different types of nonsupercell tornadoes. In the meantime, the convergence-forced updrafts produce cumulus clouds over the convergence line. In the developing stage, the cumulus clouds continue to form, while low-level small vortices propagate along the convergence line. These vortices then interact and merge with each other to create a misocyclone within which landspouts or waterspouts ultimately develop. These vortices derive their vertical vorticity mainly from the stretching of the preexisting vertical vorticity by $\partial w / \partial z$ term in the vertical vorticity equation; although the vertical tilting of baroclinically induced horizontal vorticity may also help enhance the low-level vorticity of initial vortices. In the mature stage, one of the vortices, such as vortex C, is collocated with the adjacent updraft of a towering cumulus by vorticity stretching due to convection.

11.5.3 Tornado vortex dynamics

In the developing stage of a tornado vortex, a spiral updraft strengthens from the near-surface inflow to the base of the funnel cloud. The vortex circulation is invisible below the funnel cloud unless there is dust or debris. At the mature stage, the circulation surrounding the tornado vortex is rather complicated. In the following, we will qualitatitvely describe the basic tornado vortex dynamics. Conceptually, the flow structures of the tornado vortex circulation may be classified into four major regions (Fig. 8.29). Region Ib is the *tornado core*, which surrounds the rotating axis of the tornado vortex and extends out to the radius of maximum tangential wind. The core is approximately in solid-body rotation. Region Ia is

the *outer flow*, which consists of converging air. Region II is the *boundary layer*, where the frictional force destroys the cyclostrophic flow balance (i.e. the balance between the pressure gradient force and centrifugal force). The net inward force of these three forces drives strong radial inflow into Region III, which is the *corner flow* region, where a strong updraft is produced and flows into the tornado core. Region IV is the *buoyant updraft*, which caps the vortex within the parent cloud. Tornado vortex dynamics have been studied extensively since the 1970s via observations, theories, tornado vortex chamber experiments and numerical modeling simulations.

Flow regime of the vortex circulation changes as the *swirl ratio* ($S = v_c / w_c$ at the radius of updraft or core radius r_c, where v_c is the tangential velocity of the inflow at r_c, and w_c is average vertical velocity of the updraft at the domain top) increases. If S is very small, then a one-cell vortex is formed (Figs. 8.30a and 8.30b). Note that *boundary layer separation*, as discussed in subsection 5.4.2, occurs in the corner flow for a viscous fluid with a very small swirl ratio (Fig. 8.30a). When the swirl ratio increases to a moderate value, the dynamic low pressure associated with the vortex near the rotation center, as indicated by (8.4.10), may induce a downward motion due to the strong downward pressure gradient force. At this point, a *vortex breakdown* occurs above the surface (Fig. 8.30c). For a slightly higher S, the vortex breakdown stagnation point is very close to the ground (Fig. 8.30d). When the swirl ratio increases to a large value, a turbulent two-cell vortex impinges on the groud (Fig. 8.30e), and when the swirl ratio is very large, multiple vortices may form about the annulus separating the two cells in a two-cell vortex (Fig. 8.30f).

The formation of a downdraft near the center of rotation and a two-cell vortex during vortex breakdown may be understood qualitatively by the following argument (Rotunno 1984). In an inviscid, adiabatic, homogeneous flow, the vertical momentum equation, (7.3.8) or (8.4.2), reduces to

$$\frac{Dw}{Dt} = -\frac{1}{\rho_o}\frac{\partial p}{\partial z}. \qquad (8.5.1)$$

Taking $\partial / \partial r$ of the above equation and using the cyclostrophic flow relation

$$\frac{v^2}{r} = \frac{1}{\rho_o}\frac{\partial p}{\partial r}, \tag{8.5.2}$$

leads to

$$\frac{\partial}{\partial r}\left(\frac{Dw}{Dt}\right) = -\frac{\partial}{\partial z}\left(\frac{v^2}{r}\right). \tag{8.5.3}$$

Thus, the vertical acceleration decreases toward the center of rotation when the tangential velocity decrease with height. In reality, the boundary layer dynamics cannot be ignored, since its influence helps to produce the flow in the boundary layer and corner flow regions (Figs. 8.29). The four different flow regions of a tornado vortex, as mentioned above, may be understood by considering a few special solutions, such as the steady state, for the above set of equations.

In the boundary layer away from the axis of rotation (Region II of Fig. 8.29), an inbalance between the inward pressure gradient force and the reduced centrifugal force causes the surface friction to retard the rotating flow and induce a radial inflow within the boundary layer. A tornado's boundary layer has a depth of about 100 m. Since the buoyant updraft of a tornado vortex (Region IV of Fig. 8.29) is embedded in the parent storm, the dynamics of the buoyant updraft are therefore strongly influenced by those of the parent storm.

In the boundary layer near the axis of rotation, the radial inflow associated with the secondary circulation produces strong convergence and then a vertical jet due to mass continuity. This region is called the *corner flow* (Region III in Fig. 8.29). With a laminar flow, the details of the corner flow are rather sensitive to the constant eddy viscosity coefficients used. In other words, the corner flow associated with the tornado vortex is quite sensitive to turbulence. Figure 8.31 shows one example of the effect of turbulence in a large eddy simulation of a tornado vortex with a high swirl ratio. The instantaneous pressure and vertical velocity near the surface at a height of $r_c = 0.2$, where r_c is the core

radius (e.g. 200 m), are shown. A large amount of turbulent kinetic energy is contained in the region. Several (seven in this case) secondary vortices rotating about the main vortex are clearly depicted in the figure. The strong updraft and downdraft couplet associated with each secondary vortex is largely due to its tilt. These secondary vortices provide a net angular momentum transport directed inward into the center because the vortex flow is nearly a solid body rotation so the angular momentum increases outward.

References

Barnes, S. L., and C. W. Newton, 1986: Thunderstorms in the synoptic setting. *Thunderstorm Morphology and Dynamics*, E. Kessler (Ed.), University of Oklahoma, 75-112.

Benjamin, T. B., 1968: Gravity currents and related phenomena. *J. Fluid Mech.*, **31**, 209-248.

Browning, K. A., 1964: Airflow and precipitation trajectories within severe local storms which travel to the right of the winds. *J. Atmos. Sci.*, **21**, 634-639.

Browning, K. A., and G. B. Foote, 1976: Airflow and hail growth in supercell storms and some implications for hail suppression. *Quart. J. Roy. Meteor. Soc.*, **102**, 499-534.

Browning, K. A., J. C. Fankhauser, J.-P. Chalon, P. J. Eccles, R. G. Straugh, F. H. Merrem, D. J., D. J. Musil, E. L. May, and W. R. Sand, 1976: Structure of an evolving hailstorm, Part V: Synthesis and implications for hail growth and hail suppression. *Mon. Wea. Rev.*, **104**, 603-610.

Byers, H. R., and R. R. Braham, Jr., 1949: *The Thunderstorm*. U. S. Government Printing Office, Washington, D. C., 287pp.

Chisholm, A. J., and J. H. Renick 1972: The kinematics of multicell and supercell Alberta hailstorms. Alberta Hail Studies, Research Council of Alberta Hail Studies, Rep. 72-2, Edmonton, Canada, 24-31.

Davies-Jones, R. P., 1984: Streamwise vorticity: The origin of updraft rotation in supercell storms. *J. Atmos. Sci.*, **41**, 2991-3006.

Davies-Jones, R. J. Trapp, and H. B. Bluestein, 2001: Tornadoes and tornadic storms. *Severe Convective Storms.*, C. A. Doswell (Ed.), Meteor. Monogr., **28**, Amer. Meteor. Soc., 167-221.

Doswell, C. A. III, 2001: *Severe Convective Storms.* Meteor. Monogr., **28**, Amer. Meteor. Soc., 561pp.

Fovell, R. G., and P.-H. Tan, 1998: The temporal behavior of numerically simulated multicell-type storms. Part II: The convective cell life cycle and cell regeneration. *Mon. Wea. Rev.*, **126**, 551-577.

Fujita, T. T., and R. M. Wakimoto, 1983: Microbursts in JAWS depicted by Doppler radars, PAM, and aerial photographs. Preprints, 21st Conf. on Radar Meteorology, Edmonton, Canada, Amer. Meteor. Soc., 638-645.

Gilmore, M. S., and L. J. Wicker, 1998: The influence of midtropospheric dryness on supercell morphology and evolution. *Mon. Wea. Rev.*, **126**, 943-958.

Igau, R. C., M. A. LeMone and D. Wei. 1999: Updraft and downdraft cores in TOGA COARE: Why so many buoyant downdraft cores? *J. Atmos. Sci.,* **56**, 2232–2245.

Jorgensen, D. P., and Margaret A. LeMone. 1989: Vertically velocity characteristics of oceanic convection. *J. Atmos. Sci.*, **46**, 621–640.

Klemp, J. B., 1987: Dynamics of tornadic thunderstorms. *Annu. Rev. Fluid Mech.*, **19**, 369-402.

Klemp, J. B., R. B. Wilhelmson, P. S. Ray, 1981: Observed and numerically simulated structure of a mature supercell thunderstorm. *J. Atmos. Sci.*, **38**, 1558–1580.

Lemon, L. R., and C. A. Doswell III, 1979: Severe thunderstorm evolution and mesocyclone structure as related to tornadogenesis. *Mon. Wea. Rev.*, **107**, 1184-1197.

Lewellen, W. S., 1976: Theoretical models of the tornado vortex. Proc. Symp. On Tornadoes: Assessment of Knowledge and Implications for Man, Lubbock, TX, Texas Tech University, 107-143.

Lewellen, W. S., 1993: Tornado vortex theory. *The Tornado: Its Structure, Dynamics, Prediction, and Hazards* (Church et al., eds). Amer. Geophys. Union, *Geophys. Monogr.*, **79**, 19-40.

Lewellen, D. C., W. S. Lewellen, and J. Xia, 2000: The influence of a local swirl ratio on tornado intensification near the surface. *J. Atmos. Sci.*, **57**, 527-544.

Lilly, D. K., 1986: The structure, energetics and propagation of rotating convective storms. Part II: Helicity and storm stabilization. *J. Atmos. Sci.*, **43**, 126-140.

Lin, Y.-L., and L. E. Joyce, 2001: A further study of the mechanisms of cell regeneration, propagation, and development within two-dimensional multicell storms. *J. Atmos. Sci.*, **58**, 2957-2988.

Lin, Y.-L., R. L. Deal, and M. S. Kulie, 1998: Mechanisms of cell regeneration, development, and propagation within a two-dimensional multicell storm. *J. Atmos. Sci.*, **55**, 1867-1886.

Maddox, R. A., 1976: An evaluation of tornado proximity wind and stability data. *Mon. Wea. Rev.*, **104**, 133-142.

Market, P., A. Allen, R. Scofield, R. Kuligowski, and A. Gruber, 2003: Precipiation efficiency of warm-season Midwestern mesoscale convective systems. *Wea. Forec.*, **18**, 1273-1285.

Markowski, P. M., J. M. Straka, and E. N. Rasmussen, 2002: Direct Surface Thermodynamic Observations within the Rear-Flank Downdrafts of Nontornadic and Tornadic Supercells. *Mon. Wea. Rev.*, **130**, 1692-1721.

Newton, C. W., 1966: Circulations in large sheared cumulonimbus. *Tellus*, **18**, 699-712.

Parker, M. D., and R. H. Johnson, 2004: Structures and dynamics of quasi-2D mesoscale convective systems. *J. Atmos. Sci.*, **61**, 545-567.

Proctor, F. H., 1989: Numerical simulation of an isolated microburst. Part II: Sensitivity experiments. *J. Atmos. Sci.*, **46**, 2143-2165.

Rotunno, R., 1984: An investigation of a three-dimensional asymmetric vortex. *J. Atmos. Sci.*, **41**, 283-298.

Rotunno, R., and J. B. Klemp, 1982: The influence of the shear-induced pressure gradient on thunderstorm motion. *Mon. Wea. Rev.*, **110**, 136-151.

Rotunno, R., J. B. Klemp, and M. L. Weisman, 1988 (*RKW Theory*): A theory for strong, long-lived squall lines. *J. Atmos. Sci.*, **45**, 463-485.

Simpson, J., N. E. Westcott, R. J. Clerman, and R. A. Pielke, 1980: On cumulus mergers. *Arch. Meteor. Geophys. Bioklim.*, Ser. **A29**, 1-40.

Thorpe, A. J., M. J. Miller, and M. W. Moncrieff, 1982: Two-dimensional convection in nonconstant shear: a model of mid-latitude squall lines. *Quart. J. Roy. Meteor. Soc.*, **108**, 739-762.

Trapp, R. J., G. J. Stumpf, and K. L. Manross, 2005: A reassessment of the percentage of tornadic mesocyclones. *Wea. Forec.*, **20**, 680-687.

Trapp, R. J., E. D. Mitchell, G. A. Tipton, D. W. Effertz, A. I. Watson, D. L. Andra Jr., and M. A. Magsig, 1999: Descending and nondescending tornadic vortex signatures detected by WRS-88Ds. *Wea. Forec.*, **14**, 625-639.

Wakimoto, R. M., 1985: Forecasting dry microburst activity over the High Plains. *Mon. Wea. Rev.,* **113**, 1131-1143.

Wakimoto, R. M., and J. W. Wilson, 1989: Non-supercell tornadoes. *Mon. Wea. Rev.*, **117**, 1113-1140.

Wakimoto, R. M., W.-C. Lee, H. B. Bluestein, C.-H. Liu, and P. H. Hildebrand, 1996: Eldora observations during VORTEX 95. *Bull. Amer. Meteor. Soc.*, **77**, 1465-1481.

Weisman, M. L., 1992: The role of convectively generated rear-inflow jets in the evolution of long-lived mesoconvective systems. *J. Atmos. Sci.*, **49**, 1826-1847.

Weisman, M. L., and J. B. Klemp, 1982: The dependence of numerically simulated convective storms on vertical wind shear and buoyancy. *Mon. Wea. Rev.*, **110**, 504-520.

Weisman, M. L., and R. Rotunno, 2004: "A theory for strong long-lived squall lines" revisited. *J. Atmos. Sci.*, **61**, 361-382.

Wicker, L. J., and R. B. Wilhelmson, 1995: Simulation and analysis of tornado development and decay within a three-dimensional supercell thunderstorm. *J. Atmos. Sci.*, **52**, 2675-2703.

Xue, M., K. K. Droegemeier, V. Wong, A. Shapiro, K. Brewster, F. Carr, D. Weber, Y. Liu, and D.-H. Wang, 2001: The Advanced Regional Prediction System (ARPS) - A multi-scale nonhydrostatic atmospheric simulation and prediction tool. Part II: Model physics and applications. *Meteor. Atmos. Phys.*, **76**, 143-165.

Yang, M.-J., and R. A. Houze, Jr., 1995: Multicell squall line structure as a manifestation of vertically trapped gravity waves. *Mon. Wea. Rev.*, **123**, 641-661.